BMFT-FB W 78-03

Bundesministerium für Forschung und Technologie

Forschungsbericht W 78-03

Luft- und Raumfahrt
- Weltraumforschung/Weltraumtechnologie

Time delay occultation data of the Helios spacecraft for probing the electron density distribution in the solar corona

von

P. Edenhofer

E. Lüneburg

Institut für Flugfunk und Mikrowellen der DFVLR
Oberpfaffenhofen

P. B. Esposito

W. L. Martin

A. I. Zygielbaum

Jet Propulsion Laboratory
California Institute of Technology
Pasadena, Calif.

R. T. Hansen

S. F. Hansen
High Altitude Observatory
National Center for Atmospheric Research
Boulder, Colo.

Juli 1978

Dieses Heft enthält einen Arbeitsbericht über ein vom Bundesministerium für Forschung und Technologie gefördertes Vorhaben.

Verantwortlich für den Inhalt dieses Berichtes ist der Autor.

Das Bundesministerium für Forschung und Technologie übernimmt keine Gewähr insbesondere für die Richtigkeit, die Genauigkeit und Vollständigkeit der Angaben sowie die Beachtung privater Rechte Dritter.

Als Manuskript gedruckt.

Druck, Verbreitung und Verkauf nur durch:

Fachinformationszentrum Energie, Physik, Mathematik

Gesellschaft mit beschränkter Haftung

Kernforschungszentrum

7514 Eggenstein-Leopoldshafen 2

Preis: DM 10,10

Bundesministerium für Forschung und Technologie

Forschungsbericht W 78-03

Luft- und Raumfahrt
- Weltraumforschung/Weltraumtechnologie -

Time delay occultation data of the Helios spacecraft for probing the electron density distribution in the solar corona

von

Prof. Dr. Peter Edenhofer
Dr. Ernst Lüneburg

Institut für Flugfunk und Mikrowellen der DFVLR
Oberpfaffenhofen

Dr. Pasquale B. Esposito
Warren L. Martin
Arthur I. Zygielbaum

Jet Propulsion Laboratory
California Institute of Technology
Pasadena, Calif.

Dr. Richard T. Hansen
Dr. Shirley F. Hansen

High Altitude Observatory
National Center for Atmospheric Research
Boulder, Colo.

Dezember 1977

BMFT-FB W 78-03	Abschlußbericht	Weltraumforschung/ Weltraumtechnologie

4. Titel des Berichts

Time delay occultation data of the Helios spacecraft for probing the electron density distribution in the solar corona

5. Autor(en) (Name, Vorname(n))

a) Edenhofer, Peter
Lüneburg, Ernst

b) Esposito, Pasquale B.
Martin, Warren L.
Zygielbaum, Arthur I.

c) Hansen, Richard T.
Hansen, Shirley F.

6. Abschlußdatum
Dezember 1977

7. Veröffentlichungsdatum
August 1978

9. Ber. Nr. Auftragnehmer

10. Förderungskennzeichen
BMFT-WRS Ø108/
BPT-Ø1 QC Ø46

11. Seitenzahl
48

13. Literaturangaben
49

14. Tabellen
3

15. Abbildungen
16

8. Durchführende Institution (Name, Adresse)

a) Institut für Flugfunk und Mikrowellen
der DFVLR
8031 Oberpfaffenhofen

b) Jet Propulsion Laboratory
California Institute of Technology
Pasadena, Calif. 91103

c) High Altitude Observatory
National Center for Atmospheric Research
Boulder, Colo. 80303

12. Fördernde Institution (Name, Adresse)

Bundesministerium für Forschung und Technologie (BMFT)
Postfach 120370

5300 Bonn 12

16. Zusätzliche Angaben Laufzeit-Okkultationsdaten der Sonnensonden Helios zur Sondierung der Elektronendichteverteilung in der Sonnenkorona

17. Vorgelegt bei (Titel, Ort, Datum)

18. Kurzfassung (Gliederung s. Hinweise)

S-Band Laufzeitmessungen wurden von den Sonnensonden Helios A und B während dreier solarer Okkultationen innerhalb der heliozentrischen Entfernungen von ungefähr 3 bis 215 R_O gewonnen, und zwar in Form von Entfernungsmessungen, Dopplerfrequenzverschiebungen und Elektroneninhaltsmessungen. Es wird eine Beschreibung einiger charakteristischer Merkmale der Meßverfahren und der Datenverarbeitung gegeben. Typische Datenreihen zur Sondierung der Elektronendichteverteilung nahe der Sonne (Westrand und Ostrand) mit Einschluß der äußeren und ausgedehnten Korona werden diskutiert. Stationäre und dynamische Aspekte der Sonnenkorona werden dargelegt und mit erdgebundenen K-Koronagraphen-Messungen verglichen. Unter Verwendung einer gewichteten Methode der kleinsten Quadrate werden in einer vorläufigen Analyse Parameter eines mittleren Elektronendichteprofils der Korona abgeleitet $(30/r^{6}+1/r^{2.2})\times10^{12} m^{-3}$, die zu Elektronendichten von ungefähr $1.3\times10^{11}; 1\times10^{8}; 7\times10^{6} m^{-3}$ bei r = 3; 65; 215 R_O führen. Zeitlich veränderliche Phänomene werden diskutiert und eine Ausbreitungsgeschwindigkeit v ≈ 900 km/s wird für den Plasmaausbruch eines solaren Flares bestimmt, der während einer außergewöhnlichen Meßreihe von Helios B Elektroneninhaltsmessungen am 30. April/1. Mai 1976 beobachtet wurde.

19. Schlagwörter

Helios, Okkultationen
Laufzeitmessungen
Fernerkundung
Sonnenkorona Elektronen

20.	21.	22. Preis DM 10.10

DOCUMENT CONTROL SHEET

1. Report No.	2. Type of Report	3.
BMFT-FB W 78-03	Final Report	Space Research/ Space Technology

4. Report Title
Time delay occultation data of the Helios spacecraft for probing the electron density distribution in the solar corona

5. Author(s) (Family Name, First Name(s))
a) Edenhofer, Peter
Lüneburg, Ernst
b) Esposito, Pasquale B.
Martin, Warren L.
Zygielbaum, Arthur I.
c) Hansen, Richard T.
Hansen, Shirley F.

6. Report Date
December 1977

7. Publication Date
August 1978

8. Originator's Report No.

9. Performing Organization (Name, Address)
a) Institut für Flugfunk und Mikrowellen
der DFVLR
8031 Oberpfaffenhofen
b) Jet Propulsion Laboratory
California Institute of Technology
Pasadena, Calif. 91103
c) High Altitude Observatory
National Center for Atmospheric Research
Boulder, Colo. 80303

10. BMFT-Reference No.
BMFT-WRS Ø108
BPT-Ø1 QC Ø46

11. No. of Pages
48

12. No. of References
49

13. No. of Tables
3

14. Sponsoring Agency (Name, Address)
Bundesministerium für Forschung und Technologie (BMFT)
Postfach 120370
5300 Bonn 12

15. No. of Figures
16

15. Supplementary Notes

17. Presented at (Title, Place, Date)

18. Abstract

S-band time delay measurements were collected from the spacecraft Helios A and B during three solar occultations in 1975/76 within heliocentric distances of about 3 and 215 $R_\odot$ in terms of range, Doppler frequency shift, and electron content. A description is given concerning some characteristic features of the methods of measurement and data processing. Typical data sets are discussed to probe the electron density distribution near the sun (west and east limb as well) including the outer and extended corona. Steady-state and dynamical aspects of the solar corona are presented and compared with earth-bound-K-coronagraph measurements. Using a weighted least squares estimation parameters of an average coronal electron density profile $(30/r^6 + 1/r^{2.2}) \times 10^{12}$ m^{-3} are derived in a preliminary analysis to yield electron densities of about 1.3×10^{11}; 1×10^8; 7×10^6 m^{-3} at $r = 3$; 65; 215 $R_\odot$. Transient phenomena are discussed and a velocity of propagation $v \approx 900$ km/s is determined for plasma ejecta from a solar flare observed during an extraordinary set of Helios B electron content measurements on April 30/May 1, 1976.

19. Keywords
Helios occultations
time delay measurements
remote probing
solar corona electrons

20.	21.	22. Price
		DM 10.10

Contents

1. Introduction

On December 10, 1974, and January 15, 1976, the spacecraft Helios A and B were launched fr Cape Kennedy as a joint German-American effort in the field of space re . The unique feature about the Helios mission is to approach the sun within the ecliptic plane closer than any other previous spacecraft before, the perihelion was taken to be 0.3 Astronomical Units (AU) corresponding to a value of about 65 solar radii (R_θ). This value is expected still to guarantee a safe thermal balance for the technical equipment aboard the spacecraft. The orbital period of both spacecraft is approximately half a year. Using an almost identical instrumentation for Helios A and B the scientific concept involves twelve experiments exploring basic areas in solar physics and solar-terrestrial relationships, e.g. in situ-measurements of particle densities, magnetic fields, and cosmic radiation (Porsche, 1975, 1977).

This paper deals with Helios experiment no. 12 which is essentially a radio science occultation experiment for probing the solar corona by analysing propagation effects of the spacecraft's radio signal after passage through the coronal plasma (S-band: carrier frequency 2.115 GHz uplink/2.295 GHz downlink; wave length ≈ 14 cm). Likewise spacecraft Pioneer 6 (Stelzried et al., 1970) the first part of this experiment (Volland et al., 1976, 1977) exploits the Faraday rotation effect yielding significant measurements within heliocentric distances of about 2 and 10 R_θ. The second part, reported here (also Edenhofer et al., 1977, 1977a), makes use of what is summarized as two-way time delay measurements in terms of range, Doppler frequency shift, and electron content (Martin, 1969) in order to derive the electron density distribution between about 3 and, principally, up to 215 R_θ at the earth's orbit. The lower limit is due to the increasing turbulence of the solar plasma destroying wave coherence. For Helios it turned out that the upper limit is mainly given by the orbital geometry but not by the intrinsic system noise level of the signal. From Helios B, for example, significant variations of the columnar electron content were measured as far away from the sun as approximately 190 (before) and 80 R_θ (after first inferior conjunction). Whereas Faraday rotation measurements involve the electron density and the magnetic field, time delay measurements are related only to electron densities but require precise orbital information to be analysed (at least for range and Doppler data). Both parts of this radio science experiment cover complementary aspects in probing the solar corona as far as data collection and analysis is concerned.

So it is one of the final scientific objectives to model the magnetic field by a combined data analysis of both parts of the occultation experiment. Thus in situ-measurements along the Helios trajectory and earth-bound observations of the inner corona up to about 3 R_θ (Hansen et al., 1969) are supplemented by indirect measurements from propagation effects of electromagnetic waves, remote sensing the intermediate coronal and interplanetary medium.

2. Data Collection

Similar radio science (and celestial mechanics) experiments of an occultation type have been performed to explore planetary atmospheres and the outer corona as well: Kliore et al. (1971); Rasool and Stewart (1971); Muhleman et al. (1971, 1977); MacDoran et al. (1971); Callahan (1975); Anderson et al. (1975). It is also possible to make use of solar occultations of natural, discrete radio sources: Newkirk (1967); Counselman and Rankin (1972).

2.1 Orbital Geometry

Fig. 1 shows the orbital geometry for spacecraft Helios A during 1975 as seen from the north ecliptic pole and with respect to a rotating coordinate system in which the sun-earth direction is fixed. A 5^{o}-cone for the elongation or sun-earth-probe angle (SEP) indicates the occultation situations. Time marks are given for the first perihelion, first occultation (probing the sun's west limb only: May 6, day of year (DOY) 126), and second occultation (west to east limb passage: August 31, DOY 243). For the first occultation ($SEP_{min} \approx 0.6^{o}$) the impact parameter p (distance between earth-Helios sight line and center of sun; $p_{min} \approx 2.2\ R_{\theta}$) is slowly varying ($0.6 \times 10^{-3}\ R_{\theta}/h$; value averaged over two days around occultation) as compared with the second occultation after aphelion (140 times faster). Between both occultations the rate of change for p is again minimum around July 26 ($SEP_{max} = 7.5^{o}/p = 29\ R_{\theta}$). The earth-Helios distances and the corresponding roundtrip travel times of the radio signal for the occultations are 1.8/30 and 1.5 AU/25 min, respectively. For the first occultation, figure 2 shows the earth's orbit as related to the orbit of Helios A within the ecliptic plane (orbital motion is indicated by arrows, time is shown by intervals of 10 days). The occultation position is illustrated by a broad line (alignment earth-sun-Helios), the positions for entering and leaving the 5^{o}-cone by lines (less broad) about 18 R_{θ} off the sun's west limb. Also there are marks for those time intervals corresponding to the 27-day rotational period of the sun (Carrington rotation no. 1626/dashed lines - no. 1629; also sect. 3.3).

The orbital geometry for Helios B during 1976 looks quite similar by shifting the orbit of Helios A (fig. 1) to left (east) to yield three superior cros-

sings with the earth-sun line: after first perihelion (4-15-76) there were three successive occultations on 5-16, DOY 137; 7-10; and 9-25. A value of $SEP_{max} \approx 3^{o}$ is reached around 6-8 after the exit phase of the first occultation along the sun's east limb ($p \approx 11\ R_{\theta}$). The first occultation of Helios B as seen from earth along the ecliptic plane is shown in fig. 3 (time indicated by intervals of one day); the spacecraft was behind the sun's disk for about 40 hours.

2.2 Data Acquisition

Considered with comparable interplanetary missions the Helios mission was especially suitable for solar occultation experiments due to a variety of reasons. The orbital geometry of both Helios A and B included distinct occultations (SEP $<<$ 1^{o}). There were several, successive occultations separated by weeks only (1975/76). The solar plasma could therefore be probed and compared for several rotational periods of the sun involving west and east limb observations as well. Slow and fast occultations separated time scales of plasma activity, when the Helios raypath intercepted the corona for long or short periods of time. In early May 1976 there was a special orbital configuration where a joint analysis of Helios A and B time delay data seems to be promising (the raypath of Helios A was overtaking that of Helios B). The scientific analysis of wave propagation effects is facilitated by the Helios raypath being bound to the ecliptic plane. The only latitudinal variation of solar plasma effects comes from the 7^{o} inclination of the sun's rotational axis to the ecliptic. In addition, the prime time of the Helios mission was during the descending and minimum phase of a solar cycle (no. 20 started in 1965), so conditions were quiet and stable for coronal remote sensing. Those parts of the trajectory where the earth-Helios sight line was nearly tangential support a separation of radial and angular (longitudinal) coronal probing, because the raypath was nearly constant with respect to radial variations of coronal electron densities. Since the Helios spacecraft approached the sun closer than any other spacecraft before, one can make a correlative analysis of occultation data (both time delay and Faraday rotation) with in situ-measurements. Finally, there is a very characteristic feature: on the average the Helios ranging signal was about 30 or 40 dB stronger than for missions like Mariner 6, 7, and 9. This is mainly due to a low noise, double conversion phase locked loop receiver with variable bandpass limiter and a high power mode of operation for the transponder

together with a 23 dB-high gain antenna. Thus substantially less noisy time delay data could be collected closer to the sun. Moreover for Helios B (also partly Helios A) an improved ranging machine (MU 2), especially suitable for solar occultation experiments, was available. On the other hand, a disadvantage was the lack of dual frequency capability aboard the Helios spacecraft (such as S/X-band for Mariner 10 and Vikings 1, 2).

The time delay measurements have been taken by NASA's Deep Space Network (DSN), operated by the Jet Propulsion Laboratory (JPL), California Institute of Technology, Pasadena, USA. During occultation preferably the 64-m parabolic antennas of this network were used (tracking station no. 14, California; no.43, Australia) with 100 kW of transmitted power. Away from occultation, the entire DSN including the 26-m antennas participated in the data acquisition. The notation time delay measurements means data acquisition in terms of three different data types also called radiometric data: range (roundtrip time delay), Doppler frequency shift (coherent two-way range rate), and electron content (differential phase). It is evident that the measurement technique and procedure are crucial to perform such an occultation experiment (Martin, 1969; Martin, Zygielbaum, 1977). The time delay data are determined by precisely measuring the elapsed time between the transmission of an encoded signal from the tracking station and its return, retransmitted from the spacecraft, back to the ground. A highly accurate and stable rubidium vapor oscillator, a frequency synthesizer, and a binary counter are used to generate and modulate the range signal. A range acquisition is performed by transmitting a carrier-coherent sequence of binary-coded square waves or range components (highest modulation frequency about 500 KHz ≙ fundamental time period 2 μs). By comparing the phase of the returning code with a reference based on that transmitted the roundtrip delay is determined. The Doppler frequency shift associated with the carrier is used to modify and adjust the reference phase to compensate for the two-way Doppler distortion of code phase. In order to correlate the individual range components integration times totaling 5 or 40 min were necessary depending upon the signal-to-noise ratio (SNR) in the ranging channel (with a typical system noise temperature of 25 K). While the shortest, highest-frequency range component determines the system's resolution, generally up to 9 additional components (with binary-related fractions of the fundamental frequency) were used for Helios in order to resolve range ambiguities (e.g. components no. 5: 4.56; no. 10: 146 km) adjusted to an a priori orbital fit within a certain error probability (10^{-2} or 10^{-3}). Together with the roundtrip travel time of

the signal it took up to an hour or so to obtain the value of a single range measurement(non-automatic mode of operation). Usually the strategy of the Helios radio science experimenters was to collect one or two range points at the beginning and end of a tracking pass, respectively. For a typical 8 hour-tracking pass sometimes up to 10 or 15 range measurements were collected. Range rate or Doppler data, respectively, were measured by using a sampling time of generally 60 sec.

Comparing the magnitude of the time delay measured due to the solar corona (from 0.1 to 30 μs; via differential phase even some 10 ns) to typical round-trip signal travel times of 30 min makes evident the principal requirement of utmost internal stability within the ranging system. Extensive calibration tests of the total ranging system have shown the capability to meet such a precision requirement: the order of magnitude of the long-term delay stability drifts by about 15 ns per month; the short-term stability over 5 or 8 hours drifts by about 2 ns/h with a value of 3 μs for the average delay and a standard deviation of 6 ns (Martin, 1970). Moreover it turned out that even over a 60 dB decrease in nominal signal level (20 kW) the resulting change in system delay is less than 1 ns. These numbers are certainly conservative in view of latest improvements of the ranging system. Ground tests (thermal vacuum, signal level, compatibility, etc.) showed a ranging uncertainty due to the spacecraft's transponder of less than 10 ns (Böttger et al., 1975). Operational ranging normally includes a pre- and post-track calibration. Test data results indicate that the maximum drift in the ranging system's time delay experienced over a full 8 h Helios tracking pass was less than 10 ns (0.3 % with respect to the average value of the system delay).

Electron content measurements were collected by using a special technique developed at JPL (MacDoran, Martin, 1970; MacDoran, 1970) and first applied to the Mariner 6 and 7 missions (MacDoran et al., 1971). This measurement technique is based upon the group delay and phase advance accumulated along the raypath according to wave propagation in a dispersive medium like the solar corona. Group and phase velocity $v_{g,p} \approx c(1 \mp \beta N/f^2)$ differ by the same, small amount (magnetic field and collisions neglected; c-velocity of light, β-constant, N-electron density, f-carrier frequency). Specifically, taking the resulting, opposite signed phase displacement (differential phase) in terms of the difference between the range data and the integrated Doppler data collected yields a quantity D (t) proportional to variations ΔI of the

columnar electron content I(t):

$$\Delta I(t) = I(t) - I(t_o) = \alpha\, D(t)\ ,$$
$$I(t) = \int N(s,t)\, ds \qquad [1/m^2]. \tag{1}$$

The physical meaning of the quantity D is the difference between the signal's group and phase path. Since Helios did not have dual frequency capability, the quantity $\Delta I(t)$ is an average value of the up- and down-link columnar electron content variation where the reference value $I(t_o)$ is unknown (the factor $\alpha \approx 6 \times 10^{16}$ $[1/m^3]$ depends upon the up- and down-link carrier frequency). Thus what is actually measured are variations of the electron content with respect to some reference or background level. A set of electron content measurements $\Delta I(t)$ starts at time t_o with an integration interval Δt generally equal to 2 min (for Helios B the maximum time resolution was as high as 0.5 min), i.e. discrete data values are generated at intervals of Δt. As the SNR decreased during occultation, Δt was raised to about 5 min. By comparing the phase measured during succeeding intervals with the initial determination the variations of the phase displacement are analogous to changes in the number of charged particles along the raypath. For this data type the notation DRVID has been introduced (Differenced Range Versus Integrated Doppler).

It is obvious from the concept this technique of measurement that all effects contributing to D in a non-dispersive way (independent of frequency) are cancelled. These effects include purely geometrical effects (e.g. orbital motions, antenna nutation), tropospheric propagation effects and relativistic delay, or any equipment delays common to both the range and Doppler measurement subsystem. As a consequence the data evaluation is widely decoupled from the problem of orbit determination. In a first order approximation the spacecraft's trajectory can be described by a two-body model from celestial mechanics. Contrary to the range and Doppler data, the information sensitive to the solar corona is directly accessible to a scientific analysis (i.e. comparable with a Faraday rotation type of measurement).

The basic radiometric observables are two-way coherent Doppler and range. No range acquisition can be performed without first establishing a coherent link and no electron content data can be taken without a valid range acquisition. While Doppler and range data are used precisely to determine the spacecraft's orbit, it is only the range data, however, that can provide in-

formation about absolute values for geometric range and the coronal effects. The remaining, time-dependent integration constants for the Doppler and the electron content data $I(t_o)$ are to be determined from information solely inherent to range data. After a range acquisition is completed by integrating all the lower frequency range components, the first range component is resumed in order to generate a set of electron content data starting at time $t = t_o$ as described above (post-acquisition DRVID). This set is interrupted (i.e. an abrupt, unknown change of the integration constant), whenever a new range acquisition is initiated, etc. An additional offset caused by slipping Doppler cycles due to enhanced plasma dynamics can usually be recovered by adjusting the slope of $\Delta I(t)$ across the discontinuity. Obviously a reasonable compromise had to be found in order to have long, uninterrupted sets of electron content data (e.g. 6 hours from a standard 8 h-tracking pass) and still obtain a sufficient number of range data. In terms of coronal probing this means to prefer watching for short- and long-term variations of the electron density, respectively (time scale: hours/days or weeks).

Fig. 4 gives an idea of the difficulties in establishing a coherent link and obtaining valid range acquisitions close to the sun (data taken from a previous Mariner mission). Spectral broadening of the radio signal (about 10-20 Hz for $p \approx 4\ R_\odot$) complicates the operation of both spacecraft and ground phase locked loop receivers. By monitoring the actually measured signal spectrum, it was possible, in real time, to adjust the ground receiver's bandwidth. Around occultation the spacecraft's receiver bandwidth (Böttger et al., 1975) could be set to a minimum value of about 5 Hz for adverse SNR and a bit rate of 8 bit/s (variable by steps of 8, 16, etc. up to 2048 bit/s). Sidelobes due to the quadripod supporting the Cassegrain subreflector corrupted the tracking antenna's radiation pattern causing the system noise temperature to raise to 1000 K or more during near-sun tracking. Predictions and real time measurements of this temperature were made to optimize the tracking schedule and thereby data acquisition. Real time DRVID-plots provided information on trends in plasma activity facilitating decisions to give up an electron content data set in favor of additional range data or, alternatively, to change parameters of the ranging system (e.g. integration times, number of range components) to meet sudden enhancements of the noise level. An exceptionally motivated Ranging Advisor Team (Helios B) at JPL took over such activities on a day-to-day basis during occultation optimizing equipment configurations to ensure high

quality time delay measurements.

These team efforts were enhanced by an improved ranging machine (MU 2) especially favorable to occultation type experiments and operated during the Helios mission at tracking station no. 14 (Martin, Zygielbaum, 1977). Advantages over other ranging systems include: A fully programable sequential transmission of the range components to maximize available power in each component and reduce the time required for range measurements. Only one roundtrip signal travel time per tracking pass is lost to obtain a whole set of multiple, independent range measurements (i.e. saving about 30x(n-1) min of valuable tracking time for every n range data) by "pipelining" subsequent range acquisitions in space, one after the other, also to preclude a r ndtrip time delay between measurements. Using the consistency and magnitude of the MU 2-correlation voltages (fully digitized signal processing) provided via the DSN high speed data line it was possible to assess and control the quality of the individual range measurements from real time printouts. As the raypath approaches the sun, modulation jitter of the first, shortest range component or code becomes cri- cal. The MU 2-technique allows selection of an optimal combination of any itial (e.g. 4, 8 μs, etc., instead of 2 μs) and final range component while a servo mechanism maintains the proper code alignment on the correlation voltages of all codes despite plasma induced phase shifts. It was also possible to make a redetermination of the last range measurement without interrupting a concurrent long DRVID-stretch and change the integration interval Δt to match actual noise levels. Operational error sources were reduced by automatic calibration of the radio signal phase demodulator and automatic gain control of the input signal level. Supporting a careful a posteriori analysis, it was also possible to use the correlation voltages of each range component to reconstruct the corresponding correlation functions assuming Gaussian noise to develop a combined likelihood function to be evaluated by a maximum likelihood estimator. By selecting the most probable range point of the entire acquisition an improvement of up to 1.5 dB in ranging SNR could be obtained.

As a result of all these efforts the quality and quantity of the time delay measurements from spacecraft Helios B are excellent. A total number of 141 range acquisitions was attempted within 3 weeks of May '76 (at station no. 14), about 80 % of these were found to be successful (43 pre-, 69 post-occultation range measurements). Because 16 range measurements turned out to be marginal (quality based on orbit fit), they were processed by a maximum likelihood

estimator. High flexibility made it possible in real time to respond to adverse conditions. For example, day-to-day variations of the input signal level of as much as 30 dB were observed with a 50 dB decrease over two weeks towards occultation. Maximum use could be made of the tracking time allocated to Helios and to be shared with other space projects like Viking and Pioneer in an extremely competitive situation. The acquisition of validated range data during an occultation as close to the sun as SEP = $0.84^{o}/p = 3.1\ R_{\odot}$ was never achieved before (estimated SNR for the ranging channel ≈ -15 dB) and sets a new standard in radio range system and operation performance.

3. Observations - Preliminary Analysis

The Helios A time delay measurements to be reported here cover the time interval March till September 1975. The DSN provided a total number of approximately 340 range measurements (64 m- and 26 m- stations as well). Contrary to Helios B the primary mission of Helios A did not include the first occultation, so most of the range measurements were collected just around the first and second perihelion (March plus April: 120; September: 105), i.e. the tracking coverage was supporting the entry phase of the first (5-6-75) and the (late) exit phase of the second (8-31) occultation. Unfortunately there are some bigger data gaps (ten times 4 till 7 days) and, most substantially, about 55 days amidst first occultation; coherent Doppler and range data are especially sparse during July and August. First efforts to run a precision orbit determination program in order to fit the Helios A radiometric data yielded poor results, e.g. probably more than 50 % of the range acquisitions are expected to be invalid or at least questionable. Information from station calibration data seems to be insufficient, four spacecraft maneuvers had to be taken into account. Due to difficulties in data handling and processing, about 55 MU 2-range measurements (around May/June) are not yet included in the orbit fit. So the concept was first to start the scientific orbital analysis for the Helios B spacecraft, where the overall status of this experiment looks much more promising.

3.1 Typical Data Sets

Doppler data from Helios A were analysed by Berman and Wackley (1976) to estimate parameters of an heuristic Doppler noise model for solar occultations. Fig. 5 represents the Doppler noise versus time as derived by using a data processing scheme with moving average. Usually the noise level is as low as 3 or 5 mHz

increasing to values between 0.1 and 1 Hz during occultation (numbers become questionable close to occultation). This figure gives an idea of the distinct influence of the solar corona during the slow first and the fast second occultation. Significant structures of minor peaks can be distinguished, for instance around DOY 83 (3-24) in coincidence with unusual variations of electron content measurements (sect. 3.5).

Fig. 6 shows representative time delay (roundtrip) or range (one-way) residuals from a preliminary analysis of a 2 1/2 month pre-occultation arc of Helios B radiometric data (March 1 till May 16, 1976) assuming a 3-parameter, steady-state coronal electron density model to be discussed in sect. 3.4 (a significant quantity of range data from other tracking stations, especially from no. 43, is not yet included). As is evident, some systematic trends are still present in the residuals (there is no sense to show raw data) and expected to be removed with a more detailed analysis. The solid curve gives the average coronal time delay signature. Away from occultation (SEP = 37°) a normal value is about 0.1 μs, during April and May there is a steep increase; the last eight, validated range measurements were taken on 5-13 as close to the sun as 3.1 R_θ (coronal time delay ≈ 28 μs; roundtrip signal travel time 27.3 min corresponding to 245.4×10^6 km in range). The first valid range data acquired after occultation occurred on 5-20 (3.8 R_θ/1°).

As far as electron content data are concerned there are approximately 45 sets of high quality measurements from Helios A varying between a duration of 0.5 until 6 hours. Only about 1/3 of these se[illegible] lasts longer than 3 h. The set closest to the sun (6.2 R_θ/1.7°) and still unquestionable was taken on 4-21-75 during the entry phase of the first occultation and is as short as 1.7 h. Figs. 7a,b represent two typical data sets. Elongation and impact parameter are indicated and the noise level is shown with error bars. The time scale is given in UT and local mean time. On 3-7, for example, the electron content ΔI (right scale) was measured for about 4 h, showing an increase (rate of change approximately 4.5×10^{13} m^{-2} s^{-1}) as usually expected during pre-occultation. The number of electrons along the raypath is steadily increasing towards the sun (Helios' distance to sun still 76 R_θ). Typical rates of change taken from averages on at least 2 or 3 h of observations vary like (0.7 to 50)$\times 10^{13}$ m^{-2} s^{-1}. The noise level is a low as $\sigma \approx \pm 2 \times 10^{16}$ m^{-2}. An example of unusual temporal variations for a relatively large impact parameter p = 54 R_θ is shown by a data set from 3-21 (only a few days after perihelion on 3-15). The noise level is enhanced (up to 15×10^{16} m^{-2}), typical time constants run as long as 1.5 or 2 h.

Again, for Helios B the status also for electron content measurements is better, at least from a data quantity point of view (duration of individual data sets). Fig. 8 shows Helios B electron content data taken on 5-11-76 extending as long as 6 h; the raypath's offset from the sun's west limb was only 4.8 $R_\odot$. To our knowledge there are no spacecraft supported coronal electron content measurements closer to the sun. The total variation of the electron content turns out to be approximately 0.9×10^{19} m^2, the maximum rate of change is as high as 6×10^{15} m^{-2} s^{1} (averaged over some 20 min). The excellent data quality is obvious from the noise level being as low as 0.8×10^{17} m^{-2}.

3.2 Data Processing

For indirect measurements especially from an occultation type experiment data calibration is one fundamental part of the analysis. It is understandable from sect. 2.2 that for the electron content measurements calibration is not a serious problem, at least when compared with calibrating the range data. The electron content measured via DRVID-technique has to be corrected for dispersive propagation effects contributed by that part of the signal's raypath traversing the terrestrial ionosphere. So far approximately half of the Helios A data are corrected by using a standard calibration procedure developed by Yip (1974): actual VHF-Faraday rotation measurements (California, Australia) to geostationary satellites (ATS series) are taken to derive the total electron content followed by a conversion into the desired line of sight tracking station - Helios spacecraft. A modeling computer program supposes a Chapman type ionosphere and a dipole field; differences in geomagnetic latitude are adjusted for as part of the conversion. During the Mariner 10 dual frequency mission the accuracy of this correction procedure has been demonstrated significantly to improve the navigation for spacecraft maneuvers. On 3-21 (fig. 7b), for instance, the ionospheric contribution to the variation in electron content (time resolution approximately 1/2 h) was as small as about 3×10^{16} m^{-2} within 4 of observation (for elevation angles of the tracking antenna down to 30°), whereas the total variation measured by Helios is 1.5×10^{18} m^{-2} (2 % error contribution). During the occultations of Helios A the maximum influence of the ionosphere turned out to be typically of the order of (3 to 9) $\times 10^{16}$ m^{-2} at low elevation angles. As the raypath approaches the sun, ionospheric effects become negligible in comparison to solar plasma effects. On the other hand, the ionospheric calibration procedure is important by error rates of 10 or 20 % when analysing data for quasi-statio-

nary features of the extended corona such as during pre-perihelion time intervals ($65 < p < 80\ R_\odot$) of Helios A (sect. 3.5).

The station calibration of the time delay data as outlined in sect. 2.2 introduced no critical restriction. For a full 8 h-tracking pass time delay drift and standard deviation were certainly less than 10 and 5 ns, respectively. In order to save valuable tracking time sometimes it was possible to abandon the 1/2 h post-calibration for short tracking passes. Until now the transponder calibration is accounted for only by a constant.

An essential part of the analysis of the range and Doppler data deals with the problem of orbit determination. Evidently the determination of coronal electron densities is critically dependent on a precise knowledge of the spacecraft's orbital motion, because both these types of radiometric data are taken to solve for the orbit and corona as well. A highly sophisticated double precision orbit determination program developed at JPL was used to integrate the equations of motion numerically (e.g. Moyer, 1971). The current best knowledge of the planetary and lunar ephemerides and the locations of the DSN tracking stations have been utilized in this work. So far there are at least indications for Helios B that there were no crucial problems to take into account non-gravitational forces accumulating perturbative accelerations on the spacecraft, e.g. arising from the attitude control system (spin stabilization) or the solar radiation pressure. The orbit determination problems associated with Helios A were already mentioned. Tropospheric and ionospheric corrections for propagation effects follow standard routines. From an extensive orbital analysis of space missions Anderson et al. (1975) found that for purposes of high precision orbit determination generally there is some 6 month-optimal length of data arc to be covered. hough this length may be somewhat different for the Helios B mission, it is positively due to the quantity and excellent quality of Helios B radiometric data that even a 2 1/2 month data arc yields acceptable range residuals (fig. 6) and preliminary, surprisingly good estimates of steady-state coronal parameters (sect. 3.4). So far strong evidence has been found that for Helios B the ranging accuracy seems to be limited just by plasma effects from the coronal and interplanetary medium. However, additional analysis concerning the Helios solar radiation pressure model, station and transponder calibration, and calibrations due to the turbulent corona have yet to be fully determined.

It should be noted that for relativistic perturbations affecting the space-

craft motion or the radio signal an Einstein model was used. The relativistic time delay effect (to be investigated by Helios exp. no. 11) is similar to that of the corona but much larger (e.g. Helios B prediction for 5-13: corona 20 μs/measured 28 μs; relativity 170 μs) and also different in time scale (half-decrease: 1 or 2 days; 14 days). There is abundant evidence in the literature strongly to support Einstein's theory (e.g. Anderson et al., 1975) and this implicit assumption has been made in the analysis thus far. So far no error analysis has been conducted to see how a 1 % error in the relativistic effect maps into the estimated coronal parameters (sect. 3.4). Information about standard deviations of parameters to be derived include the effect of the formal uncertainty in the gravitational theory, i.e. essentially one per cent.

For this experiment, the weighting scheme for the radiometric data as an input to the orbit determination process is especially important. Specifically, the weighting scheme decides whether or not the plasma effects inherent to the data are merely taken as noise-like statistical fluctuations of coronal electron densities or as mainly deterministic density variations in space and time. The total a priori standard deviation σ on the round trip time delay measurements is assumed to follow $\sigma_t = (\sigma_s^2 + \sigma_p^2)^{1/2}$, where $\sigma_s = 0.2$ μs ($\hat{=}$ 30 m in range) stands for a constant value of system noise and $\sigma_p = \sigma/p^{1.5}$ μs (σ = const = 33) denotes the coronal plasma noise following the "frozen turbulence" hypothesis as given by Muhleman et al. (1977). The dependence on the impact parameter p essentially corresponds to an inverse quadratic law of a steady-state coronal model (sect. 3.4); at present the values for σ_s and σ_p are given by a least squares fit to range residuals from Mariner 6, 7 data. In terms of meters (one-way) the plasma noise for the Helios observations is assumed to vary between $\sigma_p \approx 950$ and 10 m ($p = 3$ and 65 $R_\odot$). However, there is evidence that this weighting scheme is too conservative for the analysis of Helios data: Firstly, there were some substantial technical (on ground and aboard as well) and operational improvements in favor of ranging measurements for Helios B; secondly, the Mariner data were collected at a different time (solar maximum), involving different parts of the solar atmosphere (also high latitudes). A more realistic value for σ_s may be one order of magnitude smaller. Also some electron content data sets indicate that the standard deviation σ_p may be smaller, e.g. on 3-7-75 (fig. 7a) the standard deviation (related to a linear least squares fit) actually turns out to be about 0.5 m, whereas the weighting scheme takes 7.5 m ($p = 76$ $R_\odot$). For day 5-13-76, i.e. ranging closest

to the sun, it can be shown that 6 range residuals (out of a total number of 8 range acquisitions) nicely follow the temporal changes of the electron content measured and show variations of less than 100 m which is quite unusual for $p = 3.1\ R_\odot$, whereas the weighting scheme takes about 900 m. Moreover this scheme assumes that the spacecraft is always far behind the solar corona (as was indeed the case for Mariner 6 and 7). This preliminary weighting scheme for the procedure of orbit determination will be modified for Helios (e.g. taking $\sigma \neq$ const) to allow for more resolution in probing the coronal medium.

In order to derive a more realistic, refined weighting scheme for the range data in case of the Helios missions information on the actually measured variations of the electron content during an individual tracking pass is most valuable. A direct measure of these variations is given by the DRVID data (differential phase) but this data type has the disadvantage that it can be measured only after the acquisition of a range measurement. It has been demonstrated by Esposito and Lüneburg (1976/77) that the same information can be extracted directly from the Doppler residuals of a preliminary orbit determination. A constant or even linear bias in these residuals resulting from an imperfect knowledge of the orbit can be determined by fitting integrated Doppler residuals (phase residuals) with the DRVID measurements in a least squares sense. The advantage of using phase residuals is to have a better time resolution (sampling time for Doppler data often 10 s, but generally 2 min for DRVID), usually a higher accuracy (less noise from ranging modulation) and longer data stretches of electron content variation information. As an example, fig. 16 shows the agreement between the electron content variations either measured via differential phase (solid line) during a 7 h-data set or via construction from phase or integrated Doppler residuals (dotted; data set extended by about 1 h); a 20 m-offset makes the comparison more readily evident.

After subtracting the differential increase of the electron content variation as predicted (and iteratively improved) by the average steady-state electron density model due to the relative motion of earth and spacecraft with respect to this steady-state model (a purely geometrical effect) the remaining variations of the electron content measurements are assumed to reflect the turbulence characteristics of the medium. A detailed investigation of these phase fluctuations is presently carried out. The difference between the actually measured phase variations and the time average of the elctron content

variations over the whole pass at those times when ranging data have been measured form "turbulence range calibrations" and will be subtracted from the measured range value in the same way as for instance station calibrations. The variance between the calculated time average over the finite pass length and the ensemble average will provide new weights for the weighting scheme. They critically depend upon the pass length and the correlation function of the phase fluctuation.

3.3 Comparison with Ground-Based Observations of the Inner Solar Corona

An essential part of the data analysis of any solar occultation experiment is to compare the results with other information about the global structure of the corona at that time. So the scientific analysis of this experiment was prepared and started in cooperation with the High Altitude Observatory (HAO)/ National Center for Atmospheric Research, Boulder, USA. Since 1964, HAO has been carrying out a program of synoptic measurements of the intensity distribution of the sun's white light ("K") corona over the height range 1.1 - 2.7 R_θ (solar radii from sun center) with sun-eclipsing K-coronameters (Wlêrick, Axtell, 1957) from Mauna Loa, Hawaii. Azimuthal scans (steps of 5^o) are made around the solar limb at discrete heights (as many as 10) with a polarimeter, providing a two-dimensional intensity distribution in the plane of the sky of the product "pB" (polarization times brightness) which is due to Thomson scattering from electrons in the solar atmosphere. Because of the earth's orbital motion, the sun appears to rotate for the ground-based observer with a period of approximately 27 days, so that successive daily measurements can be combined to generate three-dimensional maps of the overall, large-scale intensity distribution at these various heights in the corona. In principle, pB-measurements can be deconvolved into coronal electron density models (such as discussed by Altschuler and Perry, 1972), but an entirely satisfactory, inexpensive computational program has not yet been developed. Though it is still some kind of an unsolved problem to invert pB-values via an integral relationship into electron densities, a height-dependent conversion factor can be introduced by an averaging process. Nonetheless, the raw pB-data are being used successfully for studies of short-term, transient changes (Hansen et al., 1974) as well as for studies of the longer-term evolution of magnetically-controlled structures of the inner corona (Hansen et al., 1972). These measurements can provide a basis for extrapolating optical determinations of electron density of the innermost corona (below 3 R_θ) to the much greater heights above the sun's west or east limb in the ecliptic plane where the electron content

was actually measured along the raypath to Helios spacecraft. Unfortunately, during the Helios occultations, there were no satellite-borne coronagraphs in operation; such instruments can provide information about coronal structures to distances of 6 - 10 R_θ (reviewed by Tousey, 1973).

The interpretation of the Helios time delay data as an indicator of coronal plasma conditions is greatly simplified by the fact that with the general decline of solar activity near the end of the solar cycle, the overall shape of the corona became quite stable from rotation to rotation with a nearly axially symmetric distribution as typical near solar minimum (Hansen et al., 1969, 1976; Saito, 1970; Hundhausen et al., 1976; Jager, 1959; Scheffler, Elsässer, 1974). This is illustrated in fig. 9 with a pair of isophotal maps of the coronal intensity distribution at 1.5 R_θ during November 1974 (shortly before launch of Helios A) and July 1976 (after first occultation of Helios B), as typical of the descending phase and minimum phase of the present solar cycle, respectively. An enormous simplification in the global shape is seen between those two times with the corona becoming limited to a nearly uniform, moderately bright band around the solar equator.

Fig. 10 presents the Mauna Loa K-coronal measurements in a different form. Here only the equatorial intensities are plotted (schematically), at successive limb passages around the first occultation of Helios A (starting at carrington rotation no. 1625: east/west limb data DOY 42.5/56.1 or February 11/February 25, 1975). The horizontal line represents the average coronal intensity around that time so that below-average values are indicative of coronal "holes". Dashed lines indicate times when east and west limb observations had to be combined to fill data gaps. Maximum occultation was during no. 1627 on May 6 (DOY 126) at the west limb. The stability of coronal structures is obvious as far as quiet conditions and extreme intensities are concerned, e.g. the particularly stable and intensive coronal hole around 270° solar longitude extending from the northern hemisphere of the sun for these eight solar rotations, with a longitudinal variation of ± 10 to 20°. A second, less intensive coronal hole extending from the southern hemisphere around 90 to 120° longitude existed from before rotation no. 1625 and was developing again over about six rotational periods until no. 1634, including the second Helios A occultation.

The consequences for the analysis of the Helios time delay data are evident: Conditions were most favorable to probe stationary and quasi-stationary

features of the solar corona (sect. 3.4, Fig. 11; Fig. 7a, sect. 3.5); conditions were also favorable to relate transient features of the electron content measurements (e.g. fig. 7b, sect. 3.6) to phenomena within the innermost corona generally associated with structures corotating for several solar rotational periods, as actually visible from HAO's K-coronagraph data. There is evidence that a correlation of plasma phenomena from different regions of the solar corona or interplanetary medium is useful and promising (e.g. Hundhausen, 1972; Stewart et al., 1974; Gosling et al., 1975; Hansen et al., 1976). This is also true with respect to a potential extrapolation into those regions where Helios in situ-measurements have been taken (such as data from Helios plasma experiment no. 1).

3.4 Stationary Corona

A major part of the scientific objectives of this experiment covers the derivation of the spatial and temporal distribution of coronal electron densities.

Sophisticated filter algorithms properly combined with all the relevant a priori information are necessary to derive the density distribution with a sufficient resolution from remote sensing measurements via integral relationships involving propagation effects of electromagnetic waves in inhomogeneous media like planetary and solar atmospheres (e.g. Fjeldbo, Eshleman, 1968; Kliore et al., 1971; Colin et al., 1972; Edenhofer, 1974). There are, for instance, problems of numerical instability to invert the integral equations of time delay measurements for electron densities. This is particularly true when analysing range data not only for a radial electron density profile but also for longitudinal (and much less latitudinal) coronal effects, and when analysing electron content data for effects of coronal plasma dynamics by a sequential filtering concept to probe also time variations (Pirraglia, Gross, 1970; Saito, 1970). Generally a compromise has to be balanced between numerical stability and power of resolution in space and time. Simulated Helios time delay data were analysed in a simplified computer experiment to study issues like data redundancy necessary and noise levels to be expected (Lüneburg, 1974). Presently a lengthy procedure of careful data reduction such as calibration and double precision orbit determination is still being carried out before applying inversion analyses as indicated.

As a first attempt to solve for coronal electron densities a parameterization of the problem seems to be reasonable. Following, for example, Muhleman

et al. (1971, 1977) and Anderson et al. (1975) the coronal electron density is modeled as a steady-state (time scale: months), spherically (at least axially) symmetric distribution given by a three parameter Baumbach-interpolation formula (also Scheffler, Elsässer, 1974)

$$N(r) = \frac{A}{r^6} + \frac{B}{r^{2+\varepsilon}} , \qquad (2)$$

where the quantity N denotes the electron density [m^{-3}], r the dimensionless heliocentric distance in solar radii ($r > 3\ R_\theta$), and A, B, ε are coronal parameters to be determined from the experimental data as average spatial and temporal values. The conditions holding for the measurement of the Helios time delay data such as average solar minimum, probing confined to ecliptic plane, etc. seem to strengthen the applicability of such a simplified model. No time delay measurements were collected closer than 3.1 R_θ (Helios B), where powers like r^{-16} arise dominating for $r < 1.1\ R_\theta$. The first term in (2) is expected to contribute significantly only for distances $r < 4\ R_\theta$, so the parameter A might merely be determinable from Helios B data (ranging from late entry and early exist phase of occultation as close as p = 3.1 and 3.8 R_θ, respectively). The parameters B and ε are highly correlated (table 2). The coronal electron density may vary by a factor of 2 or 3 depending on heliographic latitude (equatorial versus polar) and phase of solar cycle (Jager, 1959; Hansen et al., 1969; Scheffler, Elsässer, 1974). Density models like (2) are also used to describe an average brightness function of the white light corona. Table 1 summarizes a priori values of the coronal parameters A, B, ε as well as results from Mariners 6 and 7 as an example of previous occultation type experiments.

Table 1. Solar corona parameters

$A/10^{14}\ m^{-3}$	$B/10^{12}\ m^{-3}$	ε	
1.3 ± 0.9	1.15 ± 0.7	0.3 ± 0.3	a priori
0.69 ± 0.85	0.54 ± 0.56	0.047 ± 0.24	Mariner 6
-	0.66 ± 0.53	0.08 ± 0.24	Mariner 7

Whereas the first term of (2) - including the term r^{-16} all the more - is known also from earth-bound solar eclipse observations (e.g. coronagraph measurements), the second term with the parameters B and ε is considered to be known only with insufficient reliability ("diffuse corona") and to

vary less with solar activity (mainly observations along the earth's orbit). Due to the solar corona there is a time delay τ accumulated along the earth-Helios raypath

$$\tau = \frac{1}{c} \int \frac{1}{n} \, ds - \frac{1}{c} \int ds \ , \tag{3}$$

or equivalently, expressible in terms of the difference between the radio signal's group path and the purely geometrical distance ($n = v_g/c < 1$ is the radio refractive index of the coronal medium). Likewise for (1) it is a good approximation for S-band signal frequencies and media like the solar corona to neglect the effects of magnetic field and collisions in the dispersion relation for n. Assuming $\varepsilon = 0$ in order to get a closed, approximate expression the coronal time delay is given by

$$\tau \approx \frac{k}{f^2} \, PSE \, \left(\frac{A}{p^5} + \frac{B}{p} \right) \ , \tag{4}$$

where k is a constant and PSE denotes the probe-sun-earth angle (close to π around occultation). Thus, the time delay τ is inversely proportional to the frequency squared and to the fifth and first power of the ray's impact parameter.

With the density model (2) fully incorporated into JPL's double precision orbit determination program the problem of determining the solar corona electron density distribution is reduced to the problem of estimation of the three steady-state coronal parameters A, B, ε. The general procedure of orbit determination and weighting of radiometric data (still conservative) follows the description of sect. 3.2. In a preliminary analysis Helios B radiometric data have been analysed that were acquired within March 1 to May 16, 1976 (2 1/2 months data arc with $3 < p < 65 \, R_\theta$). The residuals (observed minus computed values) for the range and Doppler data (see also fig. 6) were formed and analysed using the classical weighted least squares algorithm (batch filter) to minimize the sum of the squares of the weighted data residuals Δz as well as weighted corrections $\Delta \tilde{x}$ to a priori estimates of the parameters. The equations for the corrections Δx to the estimated parameters and for the estimated parameter covariance matrix Λ are given by

$$\begin{aligned} \Delta x &= (A^t \, W \, A + \tilde{\Lambda}^{-1})^{-1} \, [A^t \, W \, \Delta z + \tilde{\Lambda}^{-1} \, \Delta \tilde{x}] \ , \\ \Lambda &= (A^t \, W \, A + \tilde{\Lambda}^{-1})^{-1} \ , \end{aligned} \tag{5}$$

where W is the weighting matrix, $\tilde{\Lambda}$ the a priori parameter covariance matrix, and the matrix A contains the partial derivatives of the data with respect to the unknown parameters (superscripts t and -1 mean matrix transposition and inversion, respectively). Usually the starting and a priori values for the parameter corrections are thought to be equal ($\Delta\tilde{x} = 0$); the entire process according to (5) is iterated until convergence is assured. For this preliminary analysis a basic set of 12 parameters was estimated, including: the 6 orbital elements of the Helios B trajectory (or equivalently the spacecraft's velocity components and coordinates), 3 parameters of a solar radiation pressure model (directly coupled to the equations of orbital motion), and the 3 coronal parameters of the electron density model (uncoupled from equations of motion). In addition, a set of constrained parameters adjusting to station locations, data biases, ephemeris uncertainties, etc. are being applied. When a sufficiently accurate and reliable post-flight orbit can be generated, the modeling for orbit determination will be refined, i.e. the set of parameters to be estimated will be increased step by step (possibly up to a 20 or 30-component state vector).

At present there are still data problems such as Doppler noise. After the first occultation the Helios B spacecraft continued to remain close to the sun for a long period of time. This is, for example, in contrast to the Mariner 6 and 7 trajectories, where after occultation the Doppler data quickly recovered to its original, high quality. For such a situation an improved weighting scheme to be derived from integrated Doppler residuals will certainly be of value.

A typical and preliminary solution for the coronal parameters A, B, and ε estimated from Helios B range and Doppler data as outlined above is summarized in table 2. The electron density modeled by this parameter set is shown by fig. 11 as a function of the heliocentric distance in comparison with the Mariner results (Muhleman et al., 1977).

Table 2: Preliminary estimate of coronal parameters (Helios B)

		correlation coefficients		
$A/10^{14}\ m^{-3}$	0,3	--	-0.371	-0.369
$B/10^{12}\ m^{-3}$	1,0	-0.371	--	0.998
ε	0,2	-0.369	0.998	--

So far it is impossible to present standard deviations of the coronal parameters are which can be regarded as realistic values. However, the values already obtained show clearly that the Helios B time delay occultation data are potentially very powerful for a determination of a steady-state electron density.

On the other hand, the information on the time averaged electron density profile obtained so far will be improved by constraining the weighted least squares solutions for the coronal parameters (which are principally non-unique) in such a way that reasonable mean values and standard deviations for the electron densities are attained in regions where it was impossible to collect time delay data. Close to the sun ($p < 3\ R_\odot$) HAO's coronagraph measurements can be introduced for a data fitting mainly affecting the parameter A; farer away from the sun ($p \geq 65\ R_\odot$) the Helios in situ-plasma measurements supplemented by measurements of the earth-bound IMP 7, 8 satellites (at 215 $R_\odot$) provide excellent a priori constraints to be imposed on the possible values for B and ε as supported by the estimation algorithm. Thus, for the Helios occultations there is a unique opportunity for a combined analysis of indirect and direct measurements from various sources to obtain information about the electron density distribution at heliocentric distances extending from 1.1 to 215 $R_\odot$. It is expected that such a data extrapolation is one way to reduce the averaging time intervals (i.e. subdivided lengths of data arcs or batches determining time resolution) for sets of estimated coronal parameters or resulting electron density profiles associated with corresponding radial sectors in the ecliptic plane (longitudinal corona probing).

At present some comparative remarks may be added. According to coronagraph measurements of Hansen et al. (1969) in 1964 near solar minimum an average equatorial electron density was found to be $1.4 \times 10^{13}\ m^{-3}$ for $r = 1.5\ R_\odot$. Extrapolating this value to 4 $R_\odot$ with the aid of the Helios B coronal model yields $2.5 \times 10^{11}\ m^{-3}$. For both distances Newkirk (1967) gives representative coronal electron densities (likewise equatorial values at sunspot minimum) of 1.7×10^{13} and $1.2 \times 10^{11}\ m^{-3}$, respectively, where the latter value is in agreement with the extrapolated density. For a distance of $r = 30\ R_\odot$ the value $5.6 \times 10^{8}\ m^{-3}$ from the Helios B coronal model nicely agrees with Newkirk's corresponding density of $4.6 \times 10^{8}\ m^{-3}$. Near Helios perihelion and near the earth's orbit the coronal model yields electron densities of about

10^8 and 7×10^6 m^{-3}, respectively. A comparison with the Mariner 6 coronal model needs some care. There are two basic differences: the Mariner 6 occultation ($p > 3.6$ R_θ) on 4-30-70 was during solar maximum and the orbital geometry caused the raypath to move through the full range of solar latitudes, passing over the sun's north pole for about 8 days around occultation. The determination of coronal parameters actually depends on the assumption of a spherically symmetric model for the electron density distribution (different from the Helios mission). Generally during sunspot maximum electron densities at high (low) solar latitudes are greater (smaller) than those values existing for sunspot minimum conditions (e.g. Hansen et al., 1969). To some extent the general expectation seems to be confirmed for the Mariner model to have greater (smaller) electron density values close to (farer away from) the sun ($p < 4$; $4 < p < 70$ R_θ). On the other hand, it may be questionable whether or not a latitudinal dependence of the electron density can be resolved from Helios data.

3.5 Quasi-Stationary Corona

The set of Helios A electron content measurements on 3-7-75 (fig. 7a; sect. 3.1) is taken to discuss some quasi-stationary features of the solar corona (time scale: hours or days). Fig. 12 shows the isophotal map (height 1.5 R_θ) for the corresponding Carrington rotation no. 1625 and also 1626 covering most of the entry phase of the first occultation (time runs from right to left). The global structure of the corona is illustrated by three intensity levels of contours equivalent to constant electron densities of (5.5; 7.2; 8.9) $\times 10^{12}$ m^{-3}. None of the two brightness centers (oblique lines) approximately located at solar longitudes 250° (35° S) and 100° (30° N) was intercepted by the Helios raypath indicated by a solid line from the ecliptic plane at 7° S (≈ constant during both rotational periods). However, the Helios raypath did pass through a pronounced, significant coronal hole (vertical lines) near the equator at about 70° longitude. Quite different are large-scale, long-lived coronal hole structures extending from northern and southern latitudes across the ecliptic plane around longitudes 250 and 130°, respectively (sect. 3.3). In a rough approximation now the following relationships can be established: On 3-7 (DOY 66) the elongation is about SEP = 17° and the distance earth-Helios is 0.75 AU (i.e. the signals's roundtrip travel time equals 13 min) resulting in a PSE-angle of 38°. This date of observation corresponds to a central meridian passage (CMP) date of 38°:13.2°/d ≈ 3 d earlier (DOY 63, solar longitude some 180°). As can be seen from fig. 12 this observational geometry relates to a

coronal structure which looks just like a saddle point configuration, amidst a broad band of low-leveled brightness (equivalent to electron densities of about 6×10^{12} m^{-3}) crossing the sun's equator between some 220 and 150° longitude. Though in some respects it is hypothetical to extrapolate even quiet coronal conditions from 1.5 R_θ to distances of 76 R_θ, this data set seems to be related to a time interval prevailing approximately (220°-150°):13.2°/d ≈ 5 d with a nearly uniform longitudinal distribution of coronal plasma within the ecliptic plane; there is even a good deal of latitudinal homogeneity around the Helios raypath. Thus, the linear increase of the electron content measured (6.3×10^{17} m^{-2}) should mainly be due to the radial dependence of such a quasi-stationary electron density distribution. The physical concept of such an interpretation is experimentally supported by another set of electron content data measured only two days earlier (DOY 64); this data set looks quite similar to that discussed above.

From Helios A there is a total number of 13 sets of electron content measurements (≈ 30 % of all data sets) which also vary linearly with respect to time. The correlation coefficients from a linear regression analysis are as high as 0.6 to 0.9 and even more (fig. 6a: 0.98). Most of these sets belong to the early entry and the late exit phase of occultation. There was a preference for the entry phase because of tracking coverage, noise problems, etc. Since Helios B electron content measurements could be collected closer to the sun the percentage of such "linear" data sets is smaller.

In a first order approximation a linearized approach was developed to derive a coronal parameter B from the slope of such data sets according to a density model like (2). For a physical model as simple as possible (to be described by using just one parameter) the parameter B alone describes a purely inverse quadratic law for a spherically symmetric electron density distribution. This "quadratic" coronal model is expected to hold for heliocentric distances $r > 4$ R_θ setting $A = 0$ (no Helios electron content data sets were obtained closer than $p = 5.8$ R_θ). The parameter $\varepsilon \neq 0$ means considerable complications (analytical and numerical as well), if such an exponential parameter is to be derived only from electron content data (which is even true for long arcs of range and Doppler data). Since physically the coronal parameter $\varepsilon = \varepsilon(r)$ accounts for the conservation of mass (time derivates neglected, i.e. stationary flux density and flux) associated with a radially dependent velocity profile (e.g. Hundhausen, 1972), an approximation $\varepsilon = \text{const} \approx 0$ may be justified for the electron content measurements: linear slopes were observed

preferably at the beginning of the entry phase of occultation ($p > 20$ or $30\ R_\theta$) where the velocity is still nearly constant with respect to r (e.g. 400 km/s, slowly decreasing towards occultation in those plasma regions around the raypath closest to the sun); the time interval to measure a data set is too short (less than 8 h) to yield significant radial velocity variations from the geometry of a Helios-like orbital configuration. Even from an analysis of months of data arcs the ε-values actually derived turned out to be small ($\varepsilon = 0.05$/Mariner 6; 0.2/Helios B, preliminary). Taking such a quadratic model corona and neglecting refractive effects (fully consistent with the assumption $A = 0$) yields an analytical expression for the total, one-way electron content I according to (1)

$$I = \bar{I} \times \frac{1}{p} \left(\arccos \frac{p}{r_E} \pm \arccos \frac{p}{r_P}\right) , \qquad (6)$$

$$\approx \pi \bar{I} \frac{1}{p} ; \quad p \ll r_E, r_P .$$

Heliocentric distances to earth and Helios are denoted by r_E, r_P in solar radii, an a priori value $B = 1.15 \times 10^{12}\ m^{-3}$ (table 1) gives the order of magnitude for $\bar{I} = B\ R_\theta = 8 \times 10^{20}\ m^{-2}$. The plus-sign (after perihelion) combines the contributions to the electron content along the raypath from the earth to the point of closest approach to the sun (heliocentric distance p) and from this point to the spacecraft. For small values of the impact parameter p as typical for a solar occultation the electron content I essentially depends on p only, i.e. variations of the electron content (~ integrated density) can be probed farer away from the sun than the associated density variations. Assuming a quasi-stationary corona as outlined (B = constant with respect to time) and referring to some reference time t_o, the time variations of the electron content $\Delta I(t) = I(t) - I(t_o)$ turn out mainly to be due to the time variations of geometrical quantities like $p = p(t)$ and $r_p = r_p(t)$ which can be approximated for occultation as linear functions of time with sufficient accuracy for observation intervals no longer than some hours ($\dot{r}_E \ll \dot{r}_P, \dot{p}$). Truncation of a Taylor series expansion in terms of powers of $t - t_o$ yields

$$\Delta I(t) \approx B\ R_\theta \left[-\pi \frac{\dot{p}_o}{p_o^2} \pm \frac{\dot{r}_{Po}}{r_{Po}^2}\right] (t - t_o) , \qquad (7)$$

where dotted quantities mean differentiation with respect to time and index 0 refers to quantities for $t = t_o$ (entry/exit phase: $\Delta I \gtrless 0$). So only known geometrical quantities are involved to derive the coronal parameter B from a

linear rate of change of electron content data. On the other hand, if sets of electron content measurements show a time variation which is essentially linear (where the correlation coefficient is an appropriate criterion), then the expectation is that something like a quadratic spatial decay may be a useful approximate model for an electron density distribution to start with.

Fig. 13 shows a typical example for the diurnal variation of the electron content as computed by using the exact relationship (6) for the Helios A orbit on 3-6-75. Even on a full 24h- time scale the orbital geometry gives no significant deviation from a linear slope. One day earlier and later actual 3h- and 4h- data sets of electron content measurements could be obtained (indicated by solid lines) with correlation coefficients for a linear functional dependence as high as 0.98. The slopes of these data sets were determined by a least squares fit to yield about 62×10^{12} and 45×10^{12} $m^{-2}s^{-1}$ (straight line in fig. 7a); a priori values of B yield some 6×10^{12} $m^{-2}s^{-1}$. Owing to the high Helios SNR the uncertainty associated with these slopes is as low as $\pm 10^{12}$ $m^{-2}s^{-1}$; the ionospheric influence is already corrected for. For instance, according to (6) a preliminary value of 6.3×10^{12} m^{-3} was derived (3-7) for a coronal parameter B in terms of a quasi-stationary electron density distribution. In order to get an idea of the corresponding electron density at 76 R_θ according to (2) this value can be used to give: 1.1×10^{9} m^{-3} ($\varepsilon = 0$); 3×10^{8} (0.3; a priori); 1.3×10^{8} (0.5; Scheffler, Elsässer, 1974). The preliminary results for the coronal parameters from Helios B data (table 2) yield 7.3×10^{7} m^{-3} for the same distance.

It should be pointed out that so far these values are more formal. The electron content measurements from spacecraft Helios A and B indicate a distinct day-to-day variation of the slope of those data sets linearly depending on time. Thus, B-parameters derived by such a concept actually describe an overall, but essentially local coronal electron density distribution which is thought to be quasi-stationary on a time scale of some hours. Certainly these quasi-stationary B-parameters are different from the B-parameters as usually derived from an analysis of all the radiometric data covering the entire period of occultation. Generally it turns out from Helios data sets similar to fig. 7a that the quasistationary B- and N-values associated only with local coronal regions (p typically varies by about 0.3 R_θ) are too high. Analysing radiometric data from a long orbital arc results in parameters of a stationary corona averaged on a time scale of months. Obviously it is necessary, e.g., to include non-vanishing ε-values (also supported by the high correlation with the coronal

parameter B) to obtain realistic values for the electron density. However, this means to extend the time scale of the data span and to include temporal variations of the electron content deviating from linear slopes. It is expected that the parameter ε cannot be determined on a quasi-stationary time scale, i.e. the ε-values should be taken as fixed. The question is being investigated whether or not the discrepancies are fully due to the shorter averaging time intervals for the quasi-stationary values.

An illustrative summary of Helios A electron content data as a function of time around the first occultation is given by fig. 14. The variations of the electron content as measured per tracking pass are plotted in terms of a minimum, maximum, and average (cross mark) value. As an example for the noise level the error bar is given for DOY 100 $\hat{=}$ 4-10 ($p = 16\ R_\odot$: $\sigma \approx 2\times10^{17}\ m^{-2}$). Not all the passes are shown for the early entry phase; the data gaps around occultation and at the beginning of the exit phase are obvious. As some kind of a reference level the electron content is plotted as computed (solid curves) from the Helios B stationary corona model (table 2) by using (6); probably realistic uncertainty limits are indicated for the exit phase by dotted curves. The computed values refer to a different scale with the measured data atop, i.e. according to (1) the computed values are thought to be an approximation for the unknown reference quantity $I(t_o)$ associated with variations $\Delta I(t)$ generally at least about two orders of magnitude below (DOY 100 : $I(t_o) = 1.3\times10^{20}\ m^{-2}$; $\Delta I(t) \approx 10^{18}\ m^{-2}$). As compared with the corresponding background values the order of magnitude of the measured variations is on a level of some per cent or so. The dashed-dotted curves show the electron density distribution N likewise derived from the Helios B stationary corona model.

3.6 Special Events - Transient Phenomena

This preliminary analysis is completed by a brief discussion on two examples of unusual data sets from the Helios electron content measurements.

The extraordinary feature of the Helios A electron content data set on 3-21-75 $\hat{=}$ DOY 80 (fig. 7b; sect. 3.1) may roughly be related to the concurrent global structure of the white light corona (fig. 12) as follows: Assuming the strongest interference with the coronal plasma around the raypath's point of closest approach (impact parameter $p = 54\ R_\odot$, elongation angle SEP = 15°) according to $\Delta I \sim 1/p$, one should look for an unusual coronal structure

approximately belonging to a CMP date of DOY 74 during Carrington rotation no. 1625, i.e. $(90^{o}-15^{o}):13.2^{o}/d \approx 6$ d earlier. This is pretty close to the pronounced coronal hole extending at some 70^{o} longitude along the sun's equator and intercepted by the Helios raypath as already illustrated. A more detailed description is shown by fig. 15. On 3-21 the Helios A spacecraft was situated about 25^{o} beyond the west limb of the sun (in reference to the sun-earth line). Around this date the longitudinal distribution of the equatorial K-coronal intensities is indicated and divided into sectors of uniform angular width corresponding to the solar rotation on a day-to-day basis (13^{o} longitude; CMP date relative to an earth-based observer) simplifying the actual sectors of Archimedian type. As can be seen the 70^{o}-coronal hole (also fig. 10) is really closest to the Helios raypath as compared with adjacent structures of the inner corona. The total variation of the electron content measured on a time scale of 2.7 h is $\Delta I = 1.4 \times 10^{18}$ m^{-2}, i.e. some 5 % with reference to the order of magnitude of 2.6×10^{19} m^{-2} for the corresponding background electron content approximated by using the Helios B model corona. In addition to that preliminary discussions with experimenters from plasma exp. no. 1 [+]) have shown that for electron content data sets of such kind there might have been an interaction between the Helios raypath and the spiral of a stream of high speed plasma originating from a coronal hole. A detailed investigation is being carried out proving whether or not the effects measured are in fact due to regions of compressed plasma formed at the leading edge of a high speed stream (e.g. Hundhausen, 1972).

Fig. 16 refers to the phenomenon of plasma ejecta from a solar flare intercepting the raypath of Helios B on 4-30/5-1-76 and recorded via differential phase (DRVID) and phase residual (fully equivalent to each other) as an enormous variation in electron content $\Delta I = 1.7 \times 10^{19}$ m^{-2} with a maximum rate of change of about 2.2×10^{14} $m^{-2}s^{-1}$. The values of elongation and impact parameter are 6.92^{o} and 26.1 R_{θ}, respectively, the latter decreasing by 0.8 R_{θ} within the interval of observation. Taking the Helios B model corona an approximate value of the background electron content may be 2.7×10^{18} m^{-2} at maximum, i.e. only about 1/6 of the variation measured. During the first 4 h of this electron content data set the noise is small and characteristic of reasonably quiet solar conditions. The return of the data back to a background level is not evident since the pass ended while the ejecta was still within the raypath; the flare ejecta duration interecpting the raypath is in excess of 2.5 h.

[+]) private communication from Drs. R. Schwenn, M. Montgomery.

So far the observed duration of enhanced columnar electron density in the Helios-earth raypath at impact parameter of 26.1 R_θ may be interpreted in either of two ways: 1. The flare-induced disturbance led to the continuous outward streaming (as a fire hose) of a dense plasma for at least 2.5 h, or alternatively 2. the flare ejection process itself was short-lived but produced a plasma cloud having a wide range of speeds (at 26.1 R_θ) varying from a maximum of about 900 km/s (corresponding to the delay time of 402 min for the leading edge) to a minimum of less than 660 km/s (corresponding to the last Helios measurement at 652 min after flare onset).

A correlation with the optical emergence of the flare on the solar surface gives an estimation of the flare ejecta propagation speed (roughly assuming radial direction). Table 3 gives an informative survey on earth-based observations referring to this solar flare and was provided by the Space Environment Services Center, Boulder. [+])

Table 3: Solar disturbance on 4-30-76

Optical flare, importance 2 bright
start 2048 UT, maximum 2114 UT
position S 9°, W 47° from CMP
Type III radio emission, large group,
importance 3+ (8-80 mHz)
2103 to ≈ 2113 UT
Type II radio emission, ≈ 2116 to 2125 UT
Type IV continuum, 2103 to > 2400 UT

Combined with the approximate location of the on-set of the flare in the electron content data at 03:30 UT (fig. 15), 5-1-76 (i.e. implying a travel time of 6 h 42 min), and a distance estimate of 31.3 R_θ from the flare position on the solar surface to the radial intersection with the Helios B raypath, a preliminary value of the flare propagation speed may be inferred to be $v \approx 31.3\ R_\theta / 6\text{ h }42\text{ min} \approx 900$ km/s. At present it is hypothesized that the sharp rise in the electron content data at 03:30 UT coincides with the leading edge of flare ejecta. Also the minor variation immediately preceding the rapid rise may be an evidence for a shock front preceding the main body

[+]) also private communication from Dr. Dulk, UC Boulder.

of the flare ejecta (Hundhausen, 1972).

Some final remarks may be added as to the time variation of the Helios electron content data. Because of the high ranging power of the Helios spacecrafts the noise level of the electron content measurements is nearly two orders of magnitude below that from Mariners 6, 7, 9 (e.g. Callahan, 1975). So even minor time variations of the electron content data become distinguishable. Owing to the variable bandwidth of the Helios transponder (5 Hz up to about 1.3 kHz) there are also no on-board limitations as to the high frequency time resolution for the electron content data sets with a Nyquist frequency of generally 4.2 mHz as given by the sampling theorem. Obviously there are periodical structures in the data superimposed on the linear increase (or decrease) and the transient behavior as well. So the temporal variations of nearly half of the Helios A electron content measurements consistently reveal significant periodicities within a frequency range of about 0.2 (and even less) up to 3 mHz, for instance distinct frequency peaks around, e.g., 0.35; 0.9; 2 mHz, preferably on successive days. Work is in progress to extend a maximum entropy spectral and correlation analysis (e.g. Chen, Stegen, 1974; Ulrych, Bishop, 1975) already initiated for some Helios A electron content data sets. The question is being investigated whether or not wavelike plasma structures due to preferred individual modes can be identified (Hollweg, 1975). On the other hand, the Helios electron content data are being analysed to describe the statistical fluctuations in terms of power spectra especially as far as the slope is concerned as a function of the impact parameter. An analysis towards high frequency scintillations (e.g. Jokipii, 1973) is particularly supported by using the phase residual data type (sect. 3.2) with a higher Nyquist frequency (up to 50 mHz). Improving the weighting scheme of range and Doppler data by proper noise models is one aspect of application for such a statistical approach.

Finally, the information on the coronal electron density distribution obtainable from a scientific analysis of this occultation experiment may be useful to other Helios experiments such as measuring the zodiacal light (exp. no. 9). It may be possible to analyse observations of the zodiacal light closer to the sun ($p < 20\ R_\odot$) with a higher reliability, if the scattering effect due to the electrons can be corrected for, e.g. by using coronal models like (2) with parameters actually representative for the in situ-measurements during the Helios mission.

4. Conclusions

Time delay occultation data of high quality were collected in 1975/76 from the Helios A and B spacecraft as close to the sun as 3.1 R_θ (range) and 5.8 R_θ (electron content), respectively; plasma effects could be measured directly as far away from the sun as about 190 R_θ (before first inferior conjunction of Helios B). The Helios orbital geometry and the global structure of the corona during solar minimum conditions are especially in favor of remote probing the coronal electron density distribution (west and east limb as well) including the outer and extended corona. From a preliminary data analysis steady-state and dynamical features of the electron density distribution became obvious (time scale of months/hours). Three coronal parameters for an average electron density model (i.e. spatial decay in terms of inverse powers of the heliocentric distance) are determined by a weighted least squares estimation to yield electron densities of e.g.: 1.3×10^{11}; 6.3×10^{9}; 1.4×10^{9}; 1×10^{8}; 4×10^{7}; 7×10^{6} m^{-3} at distances 3; 10; 20; 65; 100; 215 R_θ. Electron content variations mainly linear with respect to time are related to an inverse quadratic power law for electron densities of a quasi-stationary corona. For typical electron content data sets there are indications that correlations may be established with earth-bound K-coronagraph measurements revealing long-lived, corotating coronal structures. Two examples of transient plasma phenomena are discussed for Helios electron content measurements on March 21, 1975, and April 30/May 1, 1976, as probably related with an equatorial coronal hole and the special event of a solar flare. The latter is associated with an electron content enhancement of about five times typical background values (at about 30 R_θ distance from sun), the corresponding velocity of propagation for flare ejecta turns out to be some 900 km/s. More detailed coronal structures are expected to result from a correlative analysis of time delay data together with Faraday rotation data and Helios in situ-measurements.

Acknowledgements

This work was supported by the Bundesministerium für Forschung und Technologie (BMFT) and the National Aeronautics and Space Administration (NASA). Gratitude is expressed to a great number of people involved with the data acquisition, processing, and analysis: G.L. Spradlin and G. Hiendlmeier representing team efforts from the Deep Space Network (DSN) and the DFVLR-Hauptabteilung Raumflugbetrieb (GSOC); D.L. Cain, Dr. R.M. Georgevic, H.N. Royden, Dr. K.W. Yip from the Tracking and Orbit Determination Sec. at JPL together with A.I. Beers, A.C. Bouck; K. Heftman, Drs. W.G. Melbourne, W. Fogy for their continuous support likewise the Helios project scientist Dr. H. Porsche and project management G. Ousley, A. Kutzer including the program management K. Käsmeier, M. Otterbein. We would also like to thank Dr. F.H. Hibberd, H. Haumer, G. Jacob, P. Schanz, Dr. M. Eckstein, M. Malchow for their efforts. Gratitude is expressed to Drs. J.V. Hollweg, H.T. Howard, D.O. Muhleman for valuable discussions. The numerical calculations were performed with the aid of the DFVLR and JPL Computing Centers.

Figures

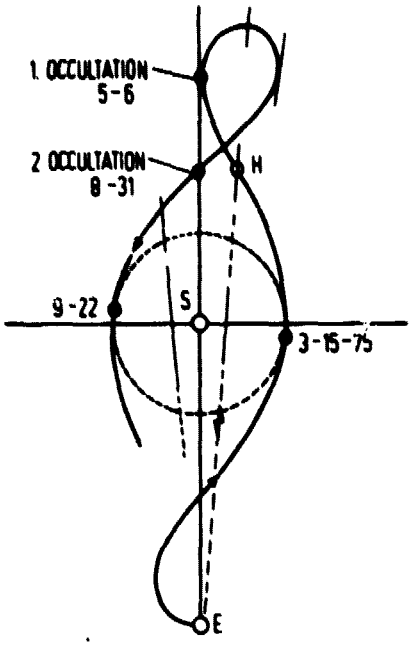

Fig. 1 Occultation geometry for spacecraft Helios A (sun-earth direction fixed)

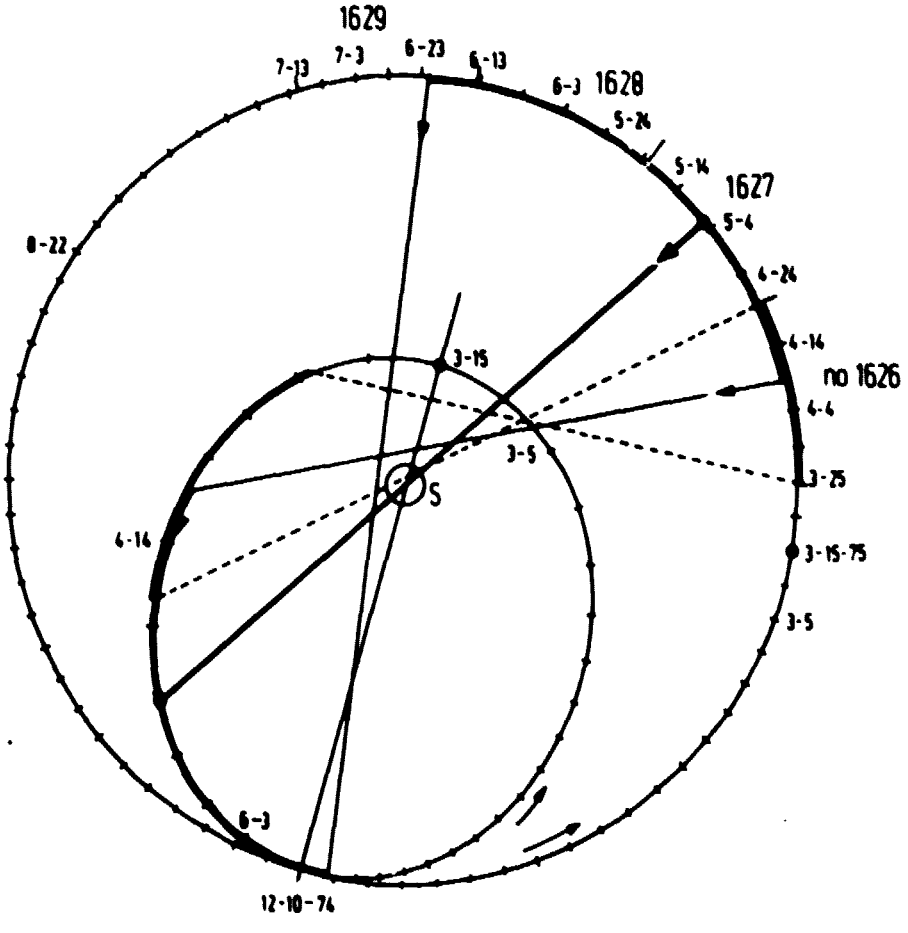

Fig. 2 Orbital geometry for first occultation of Helios A

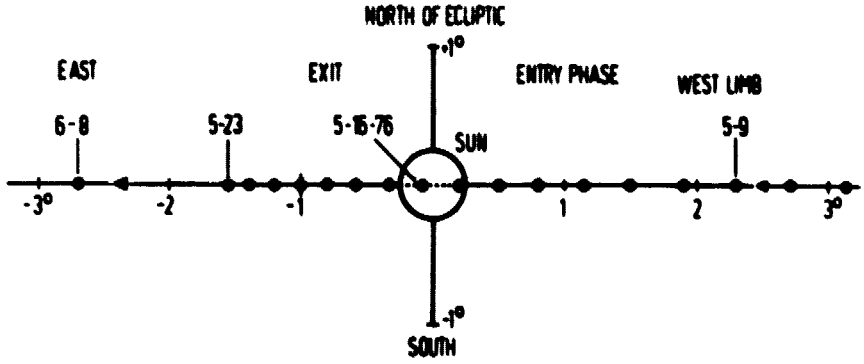

Fig. 3 Helios B trajectory behind solar disk as seen from earth (first occultation)

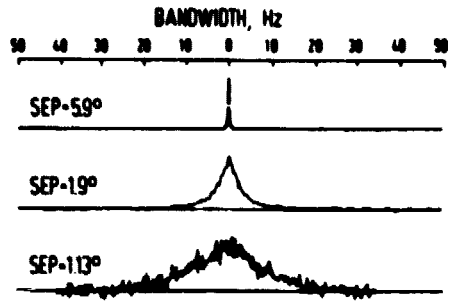

Fig. 4 Spectral distribution of the amplitude of received S-band radio signal ($1.13^{\circ} \triangleq 4.2\ R_{\odot}$)

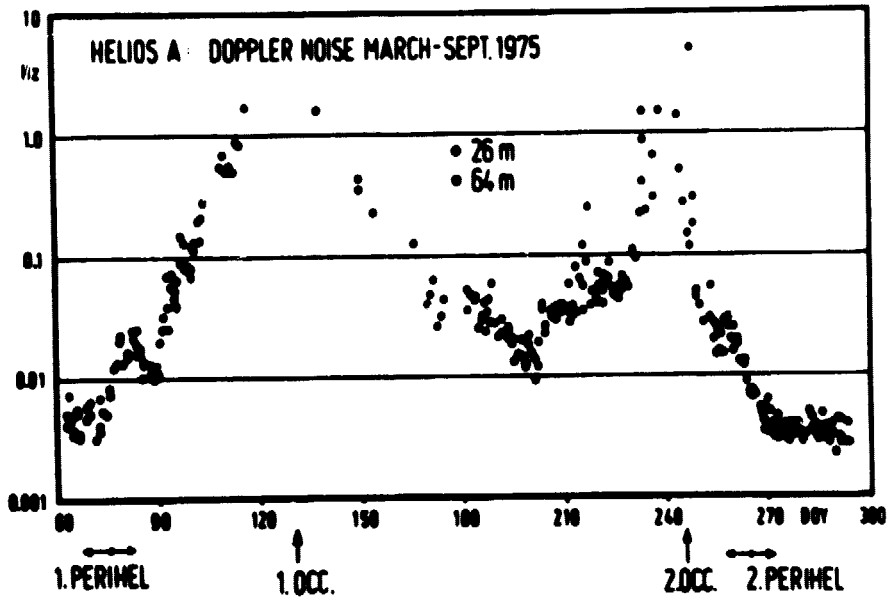

Fig. 5 Helios A Doppler noise for first and second occultation

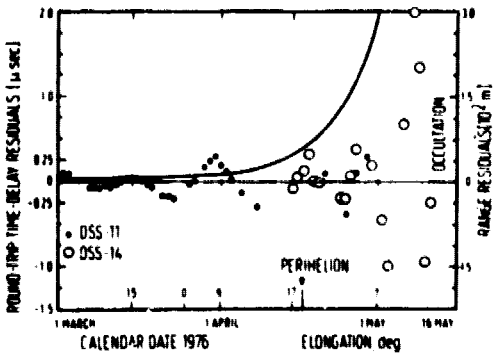

Fig. 6 Helios B range residuals and coronal time delay (entry phase of first occultation)

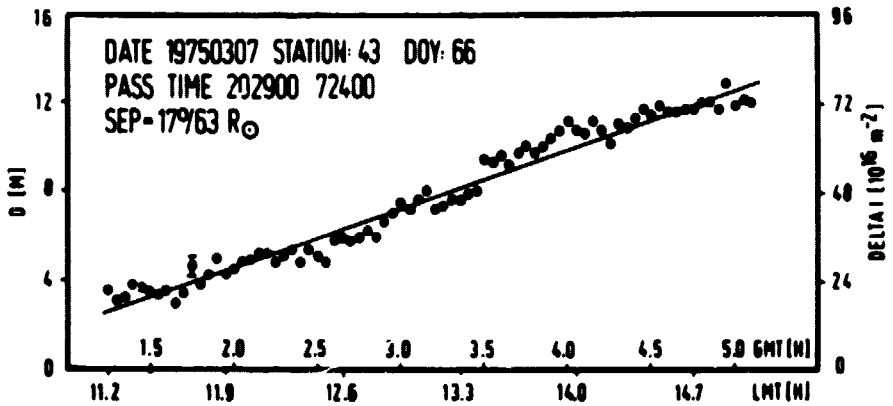

a)

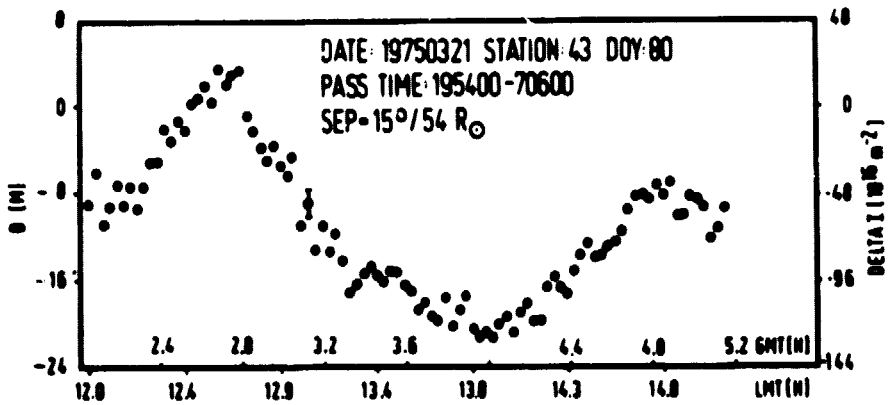

b)

Fig. 7 Helios A electron content data:
a) 3-7-75 (SEP = 17.4°); b) 3-21-75 (SEP = 14.8°)

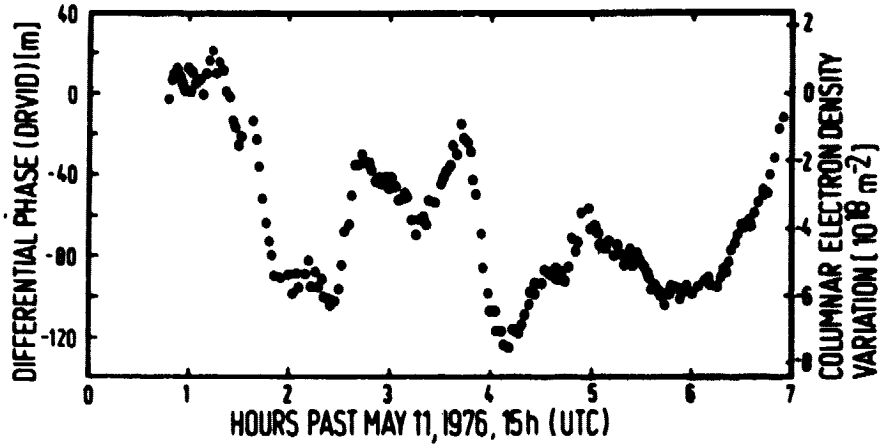

Fig. 8 Helios B electron content data closest to sun (west limb): 5-11-76 (SEP = 1.55°/p = 5.8 R_θ)

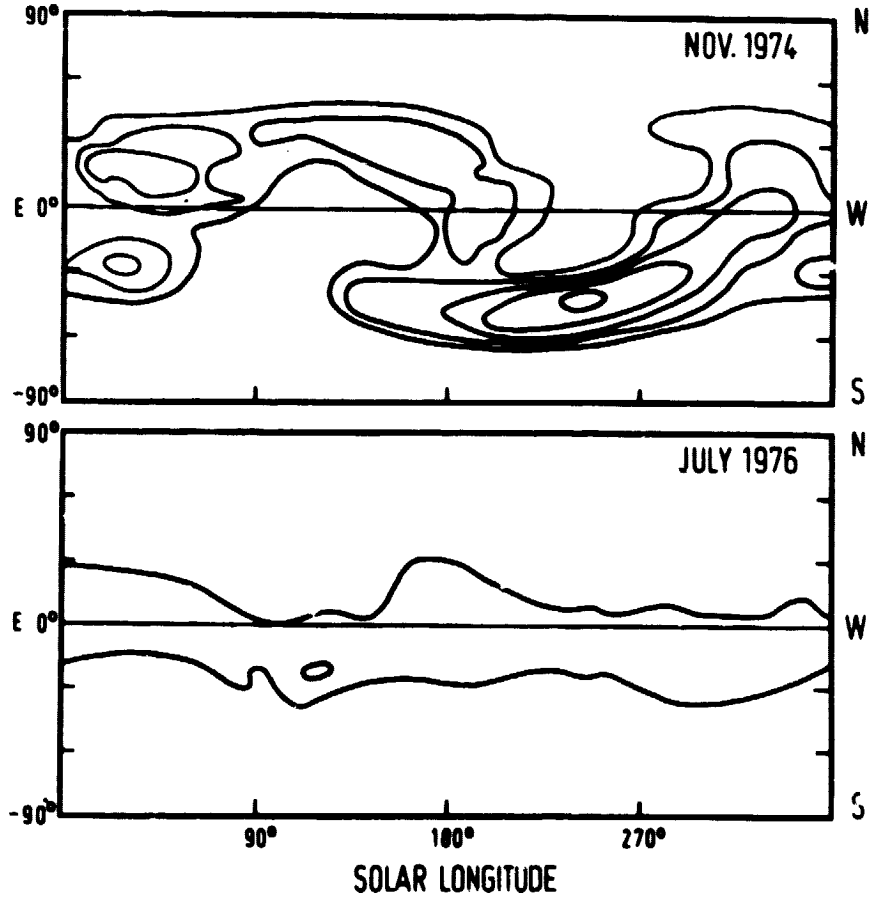

Fig. 9 Isophotal maps showing simplification of coronal structures (contours of constant pB-values at 1.5 R_θ) during descending versus minimum phase of solar cycle (1974/76)

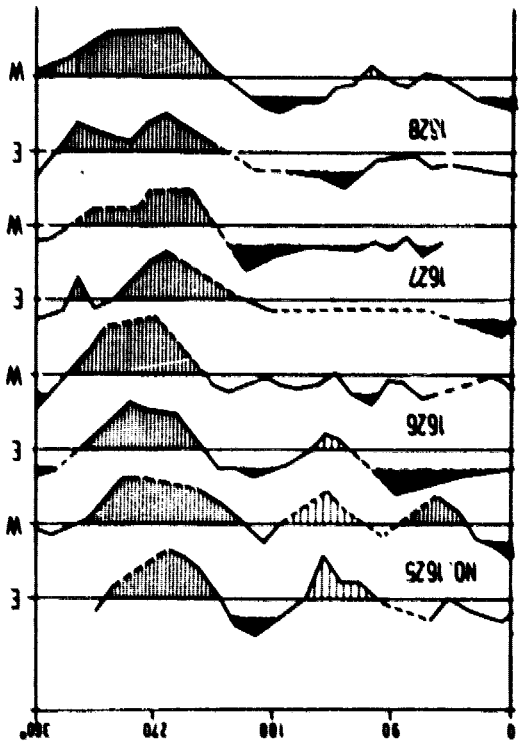

Fig. 10 K-coronal intensity at sun's equator for successive limb passages around first occultation of Helios A (four rotational periods, east and west limb)

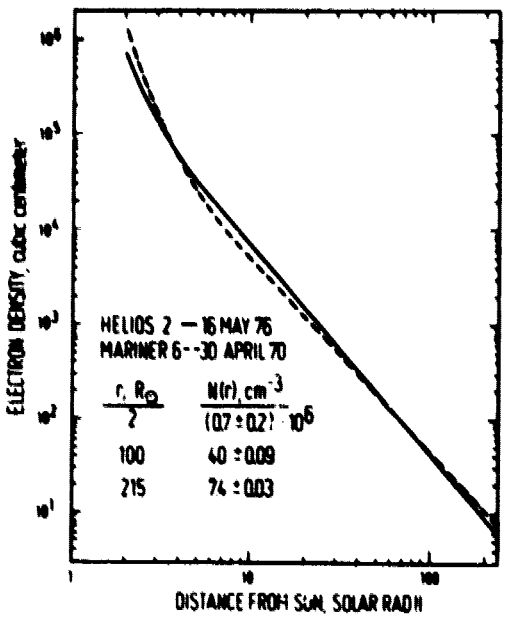

Fig. 11 Stationary coronal electron density profile (Helios B)

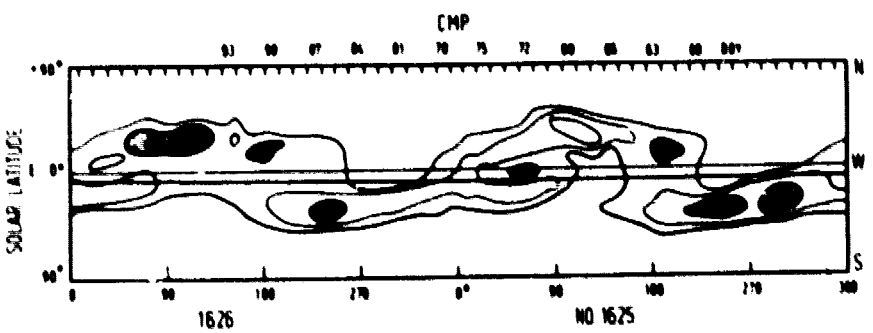

Fig. 12 Isophotal maps (CMP date) to correlate with Helios A radiometric data from March, 1975

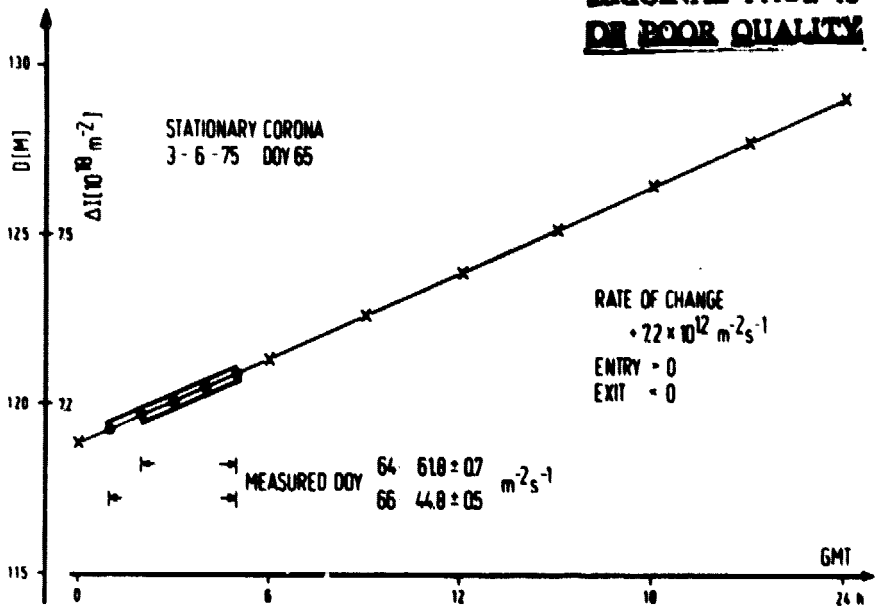

Fig. 13 Diurnal variation of electron content (quasi-stationary corona)

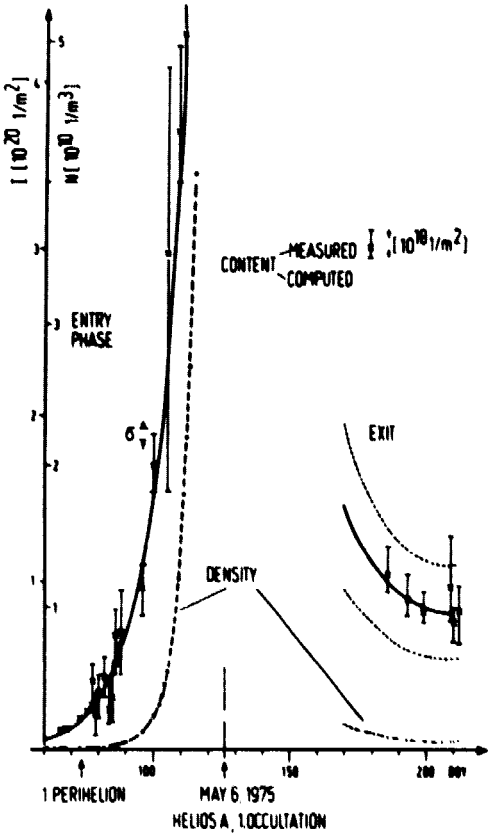

Fig. 14 Coronal electron content and density around first occultation of Helios A

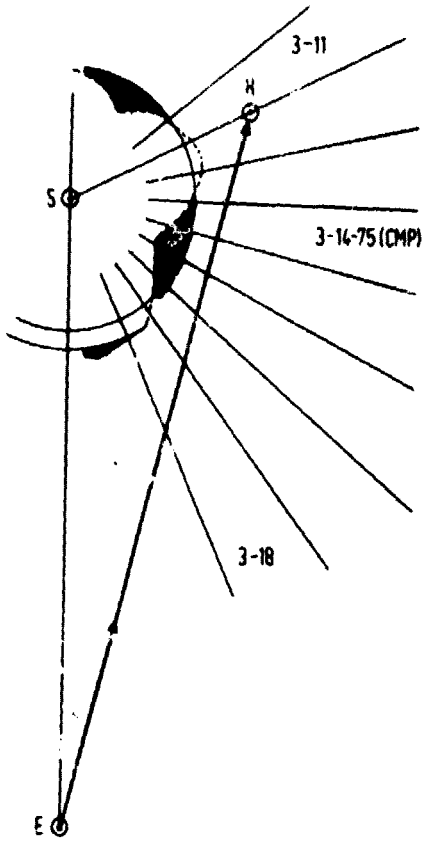

Fig. 15 Orbital geometry (sun-earth-Helios) and equatorial K-coronal intensities (west limb) around 3-21-75 (Helios A)

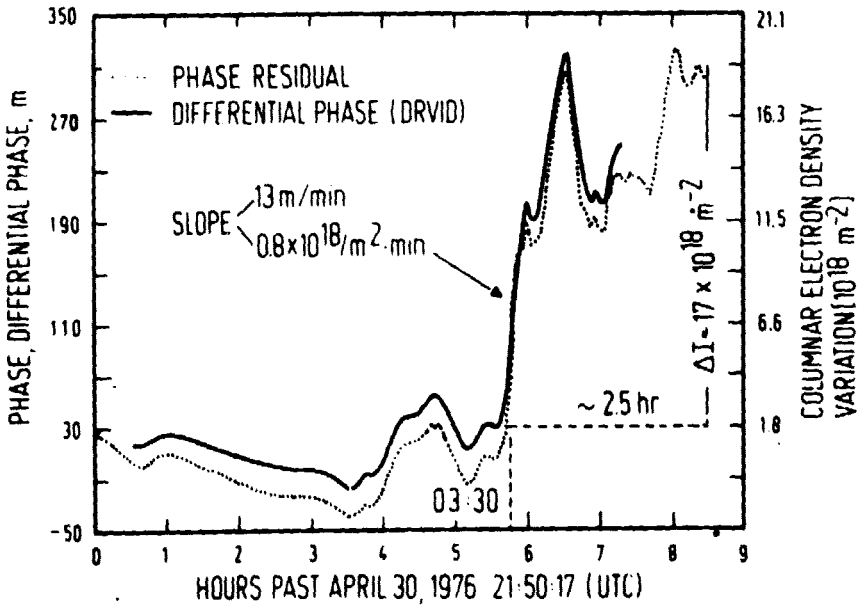

Fig. 16 Electron content variation from Helios B on 4-30/5-1-76 (flare event)

References

Altschuler, M.D., Perry, R.M.: On determining the electron density distribution of the solar corona from K-coronameter data. Solar Phys. 23, 410-428, 1972

Anderson, J.D., Esposito, P.B., Martin, W., Thornton, C.L., Muhleman, D.O.: Experimantal test of general relativity using time delay data from Mariner 6 and Mariner 7. Astrophys. J. 200, 221-233, 1975

Berman, A.L., Wackley, J.A.: Doppler noise considered as a function of the signal path integration of electron density during solar conjunctions. Inter. Mem. 412 G-76-075, Jet Propulsion Lab., California Institute of Technology, Pasadena, 1976

Böttger, H., Benöhr, H., Mann, D., Prem, H., Adamek, P.: Helios mission critical assessment of spacecraft system design goals versus actual orbit performance. Proc. IAF XXVIth Congr., Lisbon, 1975

Callahan, P.S.: Columnar content measurements of the solar-wind turbulence near the sun. Astrophys. J. 199, 227-236, 1975

Chen, W.Y., Stegen, G.R.: Experiments with maximum entropy power spectra of sinusoids. J. Geophys. Res. 79, 3019-3022, 1974

Colin, L., ed.: Mathematics of profile inversion. NASA Techn. Mem. X-62, 150, 1972

Counselman, C.C., III, Rankin, J.M.: Density of the solar corona from occultations of NP 0532. Astrophys. J. 175, 843-856, 1972

Edenhofer, P.: Inversionsmethoden bei Remote Sensing mit elektromagnetischen Wellen. Kleinheubacher Berichte 17, 343-358, 1974

Edenhofer, P., Esposito, P.B., Hansen, R.T., Hansen, S.F., Lüneburg, E., Martin, W.L., Zygielbaum, A.I.: Preliminary analysis of coronal electron content measurements from spacecraft Helios A around first solar occultation. Kleinheubacher Berichte 20, 67-80, 1977

Edenhofer, P., Esposito, P.B., Hansen, R.T., Hansen, S.F., Lüneburg, E., Martin, W.L., Zygielbaum, A.I.: Time delay occultation data of the Helios spacecrafts and preliminary analysis for probing the solar corona. J. Geophys. 42, 673-698, 1977a

Esposito, P.B., Lüneburg, E.: Correspondence between DRVID (differential phase) and integrated Doppler (phase) residuals - extension of domain of direct solar corona data. JPL Engrg. Mem. 315-4/315-10, 1-20/1-36, 1976/77

Fjeldbo, G., Eshleman, V.R.: The atmosphere of Mars analysed by integral inversion of the Mariner IV occultation data. Planet. Space Sci. 16, 1035-1059, 1968

Gosling, J.T. Hildner, E. MacQueen, R.M., Munro, R.H., Poland, A.I., Ross, C.L.: Direct observations of a flare related coronal and solar wind disturbance. Solar Phys. 40, 439-448, 1975

Hansen, R.T., Garcia, C.J., Hansen, S.F., Loomis, H.G.: Brightness variations of the white light corona during the years 1964-67. Solar Phys. 7, 417-433, 1969

Hansen, S.F., Hansen, R.T., Garcia, C.J.: Evolution of coronal helmets during the ascending phase of solar cycle 20. Solar Phys. 26, 202-224, 1972

Hansen, R.T., Garcia, C.J., Hansen, S.F., Yasukawa, E.: Abrupt depletions of the inner corona. Publications of the Astron. Soc. of the Pacific 86, 500-515, 1974

Hansen, R.T., Hansen, S.F., Sawyer, C.: Long-lived coronal structures and recurrent geomagnetic patterns in 1974. Planet. Space Sci. 24, 381-388, 1976

Hollweg, J.V.: Waves and instabilities in the solar wind. Rev. Geophys. Space Phys. 13, 263-289, 1975

Hundhausen, A.J.: Coronal Expansion and Solar Wind. 1st ed. Berlin-Heidelberg-New York: Springer 1972

Hundhausen, A.J., Hansen, R.T., Hansen, S.F., Feldman, W.C., Asbridge, J.R., Bame, S.J.: The evolution of coronal and solar wind structure in 1973 and 1974. Proc. AGU Int. Symp. on Solar-Terr. Phys., Boulder, 1976

Jager, C.: Structure and dynamics of the solar atmosphere. In: Encyclopedia of physics, Vol. LII/III, S. Flügge, ed.: pp. 80-362. Berlin-Heidelberg-New York: Springer 1959

Jokipii, J.R.: Turbulence and scintillations in the interplanetary plasma. Ann. Rev. Astr. and Ap. 11, 1-28, 1973

Kliore, A.J., Fjeldbo, G., Seidel, B.L.: Summary of Mariner 6 and 7 radio occultation results on the atmosphere of Mars. Space Research XI, 1, 165-175, 1971

Lüneburg, E.: Determination of the electron density profile of the solar corona from simulated time delay effects of Helios occultation data. Kleinheubacher Berichte 17, 359-367, 1974

MacDoran, P.F.: A first-principles derivation of the Differenced Range Versus Integrated Doppler (DRVID) charged-particle calibration method . JPL Space Programs Summary 37-62, II, 28-34, 1970

MacDoran, P.F., Martin, W.L.: DRVID charged-particle measurement with a binary-coded sequential acquisition ranging system. ibid., 34-41

MacDoran, P.F., Callahan, P.S., Zygielbaum, A.I.: Probing the solar plasma with Mariner radio tracking data. In: Proc. conf. on experimental tests of gravitation theories, R.W. Davies, ed.: pp. 105-110. JPL Techn. Mem. 33-499. Pasadena, 1971

Martin, W.L.: A binary-coded sequential acquisition ranging system. JPL Space Prog. Sum. 37-57, II, 72-81, 1969

Martin, W.L.: Performance of the binary-coded sequential acquisition ranging system of DSS 14. JPL Space Prog. Sum. 37-62, II, 55-61, 1970

Martin, W.L., Zygielbaum, A.I.: MU-2 Ranging. JPL Techn. Mem. 33-768 (in press)

Moyer, T.D.: Mathematical formulation of the double precision orbit determination program. JPL Techn. Rept. 32-1527, 1971

Muhleman, D.O., Anderson, J.D., Esposito, P.B., Martin, W.L.: Radio propagation measurements of the solar corona and gravitational field: Applications to Mariner 6 and 7. JPL Techn. Mem. 33-499, 92-104, 1971

Muhleman, D.O., Esposito, P.B., Anderson, J.D.: The electron density profile of the outer corona and the interplanetary medium from Mariner 6 and 7 time delay measurements. Astrophys. J. 211, 943-957, 1977

Newkirk, G., Jr.: Structure of the solar corona. Ann. Rev. Astr. and Ap. 5, 213-266, 1967

Pirraglia, J., Gross, S.H.: Latitudinal and longitudinal variations of a planetary atmoshere and the occultation experiment. Planet. Space Sci. 18, 1769-1784, 1970

Porsche, H.: Die Helios-Sonde als Experimenten-Träger. Raumfahrtforschung 19, 223-225, 1975

Porsche, H.: General Aspects of the mission Helios 1 and 2. J. Geophys. 42, 551-559, 1977

Rasool, S.J., Stewart, R.W.: Results and interpretation of the S-band occultation experiments on Mars and Venus. J. Atmos. Sci. 28, 869-878, 1971

Saito, K.: A non-spherical axisymmetric model of the solar K-corona of the minimum type. Annals of the Tokyo Astron. Observatory 12, 53-120, 1970

Scheffler, H., Elsässer, H.: Physik der Sterne und der Sonne. 1st ed. Zürich: Bibliographisches Institut 1974

Stelzried, C.T., Levy, G.S., Sato, T., Rusch, W.V.T., Ohlson, J.E., Schatten, K.H., Wilcox, J.M.: The quasi-stationary coronal magnetic field and electron density as determined from a Faraday rotation experiment. Solar Phys. 14, 440-456, 1970

Stewart, R.T., McCabe, M.K., Koomen, M.J., Hansen, R.T., Dulk, G.A.: Observations of coronal disturbances from 1 to 9 R_θ. Solar Phys. 36, 203-217 (I), 219-231 (II), 1974

Tousey, R.: The solar corona. Space Research XIII, 713-730, 1973

Ulrych, T.J., Bishop, T.N.: Maximum entropy spectral analysis and autoregressive decomposition. Rev. Geophys. Space Phys. 13, 183-200, 1975

Volland, H., Bird, M.K., Levy, G.S., Stelzried, C.T., Seidel, B.L.: Helios-1 Faraday rotation experiment: Results and interpretation of the solar occultation in 1975. Rept. Radioastronomisches Institut, Universität Bonn, 1-19, 1976

Volland, H., Bird, M.K., Levy, G.S., Stelzried, C.T., Seidel, B.L.: Helios-1 Faraday rotation experiment: results and interpretations of the solar occultations in 1975. J. Geophys. 42, 659-672, 1977

Wlérick, G., Axtell, J.: A new instrument for observing the electron corona. Astrophys. J. 126, 253-258, 1957

Yip, K.W.: The ionospheric calibration technique for the V075 celestial mechanics and radio science experiments. JPL Engrg. Mem. 391-606, 1-17, 1974